

Chemical Abundances in the Nuclear Star Cluster of the Milky Way: α -Element Trends and Their Similarities with the Inner Bulge

NILS RYDE,¹ GOVIND NANDAKUMAR,^{1,2} MATHIAS SCHULTHEIS,³ GEORGES KORDOPATIS,³ PAOLA DI MATTEO,⁴ MISHA HAYWOOD,⁴ RAINER SCHÖDEL,⁵ FRANCISCO NOGUERAS-LARA,⁶ R. MICHAEL RICH,⁷ BRIAN THORSBRO,³ GREGORY MACE,⁸ OSCAR AGERTZ,¹ ANISH M. AMARSI,⁹ JESSICA KOCHER,¹ MARTA MOLERO,¹⁰ LIVIA ORGLIA,¹¹ GIULIA PAGNINI,¹² AND EMANUELE SPITONI¹³

¹*Division of Astrophysics, Department of Physics, Lund University, Box 118, SE-22100 Lund, Sweden*

²*Aryabhata Research Institute of Observational Sciences, Manora Peak, Nainital 263002, India*

³*Université Côte d'Azur, Observatoire de la Côte d'Azur, Laboratoire Lagrange, CNRS, Blvd de l'Observatoire, 06304 Nice, France*

⁴*Observatoire de Paris, section de Meudon, GEPI, 5 Place Jules Janssen, 92195 Meudon, France*

⁵*Instituto de Astrofísica de Andalucía (CSIC), Glorieta de la Astronomía s/n, 18008 Granada, Spain*

⁶*European Southern Observatory, Karl-Schwarzschild-Strasse 2, 85748 Garching bei München, Germany*

⁷*Department of Physics and Astronomy, UCLA, 430 Portola Plaza, Box 951547, Los Angeles, CA 90095-1547, USA*

⁸*Department of Astronomy and McDonald Observatory, The University of Texas, Austin, TX 78712, USA*

⁹*Theoretical Astrophysics, Department of Physics and Astronomy, Uppsala University, Box 516, SE-751 20 Uppsala, Sweden*

¹⁰*Institut für Kernphysik, Technische Universität Darmstadt, Schlossgartenstr. 2, Darmstadt 64289, Germany*

¹¹*INAF, Osservatorio di Astrofisica e Scienza dello Spazio di Bologna, Via Gobetti 93/3, 40129 Bologna, Italy*

¹²*GEPI, Observatoire de Paris, PSL Research University, CNRS, Place Jules Janssen, F-92195 Meudon, France*

¹³*INAF, Osservatorio Astronomico di Trieste, Via Tiepolo 11, 34131 Trieste, Italy*

Abstract

A chemical characterization of the Galactic Center is essential for understanding its formation and structural evolution. Trends of α -elements, such as Mg, Si, and Ca, serve as powerful diagnostic tools, offering insights into star-formation rates and gas-infall history. However, high extinction has previously hindered such studies. In this study, we present a detailed chemical abundance analysis of M giants in the Milky Way's Nuclear Star Cluster (NSC), focusing on α -element trends with metallicity. High-resolution, near-infrared spectra were obtained using the IGRINS spectrograph on the Gemini South telescope for nine M giants. Careful selection of spectral lines, based on a solar-neighborhood control sample of 50 M giants, was implemented to minimize systematic uncertainties. Our findings show enhanced α -element abundances in the predominantly metal-rich NSC stars, consistent with trends in the inner bulge. The NSC stars follow the high- $[\alpha/\text{Fe}]$ envelope seen in the solar vicinity's metal-rich population, indicating a high star-formation rate. The α -element trends decrease with increasing metallicity, also at the highest metallicities. Our results suggest the NSC population likely shares a similar evolutionary history with the inner bulge, challenging the idea of a recent dominant star formation burst. This connection between the NSC and the inner-disk sequence suggests that the chemical properties of extragalactic NSCs of Milky Way type galaxies could serve as a proxy for understanding the host galaxies' evolutionary processes.

Keywords: stars: abundances, late-type – Galaxy:evolution, disk – infrared: stars

1. INTRODUCTION

In recent years, considerable effort has been devoted to reach a holistic picture of the Galactic Center region of the Milky Way. The goal is to get a better understanding of the relation between its formation history and that of the Milky Way as a whole, but also a better understanding of the roles played by galactic nuclei in galaxy formation and evolution,

in general (see, e.g. Neumayer et al. 2020; Schödel et al. 2023). A chemical characterization of this region is a critical component of this endeavor.

The center of the Milky Way consists of the Nuclear Star Cluster (NSC), the Nuclear Stellar Disk (NSD), and the Central Molecular Zone (CMZ). The NSC is a compact, spherical stellar structure with a half-light radius of ~ 4 pc, a diameter of ~ 12 pc ($\sim 300''$), and a total stellar mass of $2 \times 10^7 M_{\odot}$ (e.g. Schödel et al. 2014b,a; Feldmeier et al. 2014; Chatzopoulos et al. 2015; Fritz et al. 2016; Feldmeier-Krause et al. 2017b; Gallego-Cano et al. 2020). The surrounding NSD consists of a flat, rotating, disk-like structure

with a break radius of ~ 90 pc, a vertical height of ~ 45 pc, and a total stellar mass of $1 \times 10^9 M_{\odot}$ (see, e.g., [Launhardt et al. 2002](#); [Bland-Hawthorn & Gerhard 2016](#)). The NSD lies within the Central Molecular Zone (CMZ), which is $\sim 250 \times 50$ pc large ([Henshaw et al. 2023](#); [Schödel et al. 2023](#)) and the Galactic Center region is, as a whole, embedded in the Galactic Bulge/Bar ([Sormani et al. 2022](#)).

Large gas inflows channeled by the Galactic bar have made the Galactic Center region the largest reservoir of dense gas in the Milky Way ([Baba & Kawata 2020](#); [Sormani et al. 2022](#)). Populations of young stars provide evidence for recent star formation in the predominantly old stellar populations with ages between 8-10 Gyrs ([Matsunaga et al. 2011](#); [Nogueras-Lara et al. 2020](#); [Schödel et al. 2020](#); [Thorsbro et al. 2023](#); [Gallego-Cano et al. 2024](#)). The star-formation histories (SFH) have varied with time and appear different in the NSD and NSC ([Schödel et al. 2020](#); [Nogueras-Lara et al. 2021a](#)). While there are differences in the stellar populations and formation histories of the NSD and NSC, [Nogueras-Lara et al. \(2023\)](#) suggest, based on kinematics and metallicity gradients of the two systems, a smooth transition between the two and that they might be parts of the same structure. In the NSC, the majority of star formation was determined by [Schödel et al. \(2020\)](#) to have occurred more than 10 Gyrs ago. However, it also seems to contain an intermediate-aged population, approximately 3 Gyrs old, which accounts for less than 15% of the total star formation ([Schödel et al. 2020](#); [Nogueras-Lara et al. 2021a](#)). In contrast, [Chen et al. \(2023\)](#) identify a dominant, metal-rich component (constituting over 90% of the stellar mass) in the NSC, with an age of around 5 Gyrs.

There are two primary formation scenarios proposed for the NSC ([Neumayer et al. 2020](#)): (i) In-situ formation, where gas is funneled into the central few parsecs, triggering star formation. This process may be driven by several mechanisms, including bar-driven gas infall, dissipative nucleation, tidal compression, or magneto-rotational instability (see [Neumayer et al. 2020](#) for further discussion). (ii) Infall of massive stellar clusters into the galactic nucleus, which could account for the metal-poor population observed in the NSC (e.g., [Capuzzo-Dolcetta 1993](#); [Mastrobuono-Battisti & Capuzzo-Dolcetta 2012](#); [Hartmann et al. 2011](#); [Arca-Sedda & Capuzzo-Dolcetta 2014](#)). Indeed, recent work using cosmological zoom simulations ([Gray et al. 2024](#)) has demonstrated how metal-poor ($[Fe/H] \lesssim -1$) NSCs can form in starbursting dwarf galaxies at high redshifts, with cluster properties in agreement with observations. However, globular cluster infall cannot explain the presence of young stars (e.g., [Feldmeier-Krause et al. 2015](#)) and globular clusters observed in the Milky Way today cannot have contributed a significant fraction of the mass of old stars in the NSC ([Dong et al. 2017](#)). It is most likely that the NSC formed through a combination of both these scenarios.

Abundance trends versus metallicities for the different stellar populations in the Galactic Center can add new pieces of evidence. Such studies would complement investigations of dynamics, kinematics, star-formation histories, and the dis-

tribution of metallicities. Since different elements represent different nucleosynthetic channels with their own evolutionary timescales (see, e.g., [Matteucci 2021](#); [Manea et al. 2023](#)), the trends will be different depending on, for instance, the star-formation rate and gas infall, and can, therefore, reveal differences between stellar populations.

Detailed abundance measurements near the plane and Galactic Centre, however, still remain relatively sparse. Due to high dust-extinction ([Nishiyama et al. 2006](#); [Nogueras-Lara et al. 2018](#)), high-resolution spectroscopic observations of stars in the Galactic Center need to be carried out in the near-infrared (H and K bands) regime. Abundance trends of the Galactic Center region first appeared in [Cunha et al. \(2007\)](#). They focused on the young supergiant population in the NSC showing elevated α -elements at high metallicities. Later, [Ryde & Schultheis \(2015\)](#); [Ryde et al. \(2016a,b\)](#); [Nandakumar et al. \(2018\)](#); [Nieuwmunster et al. \(2023\)](#) presented α -element trends for 9 giants from the old population probably in the NSD and not in the NSC ($2.5 - 5.5'$ North of the very center, which corresponds to a projected galactocentric distance of $5 - 10$ pc) showing more thick-disk-like behaviour for the metal-rich stars there. A few years later, [Do et al. \(2018\)](#) derived elevated abundances of V, Sc, Y from strong spectral lines in two cool, metal-rich stars within 0.5 pc from the very center, i.e. in the NSC. These strong lines were instead explained in [Thorsbro et al. \(2018\)](#) as a line-formation property in cool giants, rather than being due to a high abundance. In the first $[Si/Fe]$ determinations for old stars actually in the NSC, [Thorsbro et al. \(2020\)](#) find a disk-like trend at subsolar metallicities, but an enhanced trend at supersolar metallicities. From a dynamical investigation, 15 of the stars investigated were determined to be located in the NSC and 5 in the NSD. The near-infrared spectroscopic survey APOGEE (Apache Point Observatory Galactic Evolution Experiment; [Holtzman et al. 2018](#); [Jönsson et al. 2018](#)) also targeted these inner regions, although only a handful of their stars lie in the projected region of the NSD¹. They determined the α -abundance trends for stars in their GALCEN field, centered at $(l, b) \sim (+0^{\circ}.2, -0^{\circ}.1)$, showing trends similar to that observed in the Galactic bulge ([Schultheis et al. 2015, 2020](#)).

The aim of the present study is to investigate the abundance trends of the α elements Mg, Si, and Ca as a function of metallicity for a sample of stars in the Nuclear Star Cluster, differentially against the trends from a control sample of the same type of stars in the solar neighbourhood (based on the study by [Nandakumar et al. 2023](#)). We will thus compare detailed abundances of M giants in both stellar populations, observed with the highest resolution infrared spectrograph available and analysed in the same way, which minimizes any possible systematic uncertainties. We search for differences that may reflect a different chemical evolution in the NSC, compared to the solar vicinity.

¹ The fibre diameter of $2''$ used in APOGEE is not adequate to study the Galactic Centre given the high stellar crowding.

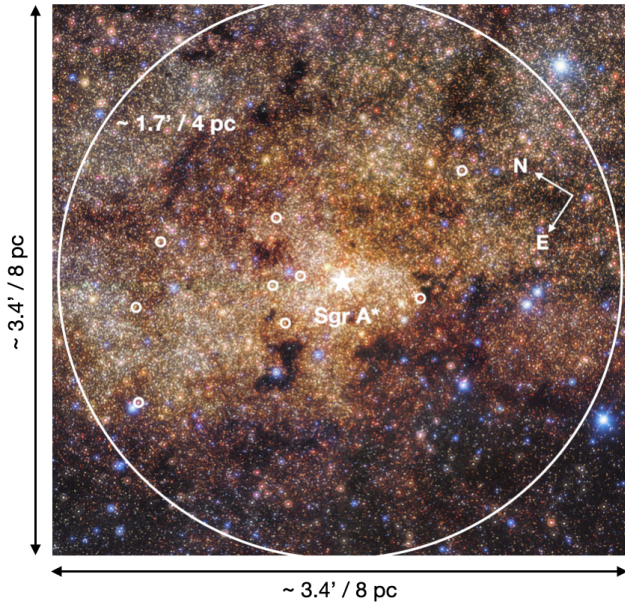


Figure 1. GALACTICNUCLEUS JHK_s image of the Milky Way’s NSC (Nogueras-Lara et al. 2018, 2019) showing the 9 stars for which we have obtained spectra, marked by white small circles. The image scale is $8 \times 8 \text{ pc}^2$ and the large white circle indicates the effective radius of the NSC ($\sim 4 \text{ pc}$, or $\sim 100''$), while the position of the supermassive black hole, A*, is denoted by a white star in the middle of the image. The directions East (E) and North (N) are labeled in the upper right corner.

This paper is the third in a series characterizing the chemistry in the intermediate-age to old red giants populations of the Galactic Center with high-resolution, near-IR spectroscopy. The first paper (Rich et al. 2017), which was based on KECK/NIRSPEC observations of 15 M giants in the NSC, found a broad metallicity distribution ranging from $-0.5 < [\text{Fe}/\text{H}] < +0.5 \text{ dex}$, with most of the stars being at or below the solar iron abundance. This is broadly similar to other fields in the Galactic bulge, and not as narrow as that found for supergiants in the NSC (Cunha et al. 2007). In the second paper (Thorsbro et al. 2018), we explore the silicon abundance trends versus metallicity for these 15 NSC stars. The trends of the α elements are diagnostically interesting and are sensitive to the star-formation rates in the stellar population. We find a thick-disk trend for subsolar metallicities, but a surprising $[\text{Si}/\text{Fe}]$ enhancement for supersolar metallicities of $+0.25 < [\text{Fe}/\text{H}] < +0.5$ in 4 NSC stars and 2 NSD stars. To confirm this result, it is necessary to study the trends of more α elements in a bigger sample of stars. We note again that Cunha et al. (2007) found enhanced alpha elements in the supergiant population, while Ryde & Schultheis (2015); Nieuwmunster et al. (2023) found trends for Mg, Si, and Ca resembling the enhanced disk trend for NSD stars. Similar results were found by Schultheis et al. (2020) for the NSD.

In this study we will, thus, present the detailed α abundances of the Nuclear Star Cluster observed at a spectral resolution that resolves stellar lines. In a forthcoming paper in the

series, we will further discuss elemental abundance trends for other groups of elements such as fluorine, odd-Z, iron-peak, and neutron-capture elements. The details of the observations and data reduction are provided in Section 2, followed by the details of the spectroscopic analysis in Section 3. In Section 4, we show the elemental abundance trends together with the identically analysed 50 solar neighborhood stars. We discuss our results in Section 5 and conclude in Section 6.

2. OBSERVATIONS AND DATA REDUCTION

We have determined the stellar parameters and the α elements for 9 M-giants ($T_{\text{eff}} < 4000 \text{ K}$) in the NSC from high-resolution spectra observed with the Immersion GRating INfrared Spectrograph (IGRINS; Yuk et al. 2010; Wang et al. 2010; Gully-Santiago et al. 2012; Moon et al. 2012; Park et al. 2014; Jeong et al. 2014). IGRINS provides spectra with a spectral resolving power of $R \sim 45,000$, spanning the full H and K bands ($1.45 - 2.5 \mu\text{m}$), thus giving access to a wealth of spectral lines enabling a detailed study of stellar abundances for a range of different elements.

The stars were observed with IGRINS mounted on the Gemini South telescope (Mace et al. 2018) under the programs GS-2022A-Q-208, GS-2023A-Q304, and GS-2024A-Q-304. These were observed in service mode over a period from May 2022 to April 2024 and their location on the sky is shown in Figure 1. The stars are presented in Table 1, where the H and K magnitudes are given, as well as the date of observation, exposure times, and achieved signal-to-noise ratio (S/N) per resolution element in the H and K bands, respectively. The Gemini Program identifications for the three runs are also provided for every star.

The IGRINS observations were conducted using one ABBA nod sequence (for the 2022, and 2023 runs) and two nod sequences (for the 2024 run) along the slit to facilitate sky background subtraction. Exposure times were chosen to achieve an average S/N of approximately 100 in the K band, resulting in observing times ranging up to 50 minutes. Despite the higher sensitivity of the IGRINS H-band detector, the significant reddening affects the H band more than the K band (Nogueras-Lara et al. 2020), resulting in lower S/N in the H band.

The IGRINS data were reduced with the IGRINS PipeLine Package (IGRINS PLP; Lee et al. 2017) to optimally extract the wavelength calibrated spectra, order by order, after flat-field correction and A-B frame subtraction (Han et al. 2012; Oh et al. 2014). The H-band spectra range from $1.45 - 1.83 \mu\text{m}$ over 27 orders, and the K-band from $1.87 - 2.49 \mu\text{m}$ over 26 orders. The wavelength solution is based on sky OH emission lines.

The contaminating telluric lines were reduced by dividing the target spectra with a telluric standard-star spectrum, showing no stellar features, in our case fast-rotating late-B to early-A dwarfs. These were observed close in time and at an air mass similar to that of the science targets. In the subsequent abundance analysis, we keep track of the spectral regions impacted by, but corrected from telluric lines ensur-

Table 1. Observational details of M giant stars.

Name ^a	RA	DEC	H ^b	K _s ^b	Date	Exp. Time	S/N _H / S/N _K ^c	id ^d	Telluric star
	h:m:s	d:m:s	[mag]	[mag]	UT	[s]	per res. element		A0V
FK48 ⁽²⁾	17:45:41.301	-29:00:08.406	12.53	10.76	2023-04-30	2240	35/105	48	HIP86098
FK5020265 ⁽²⁾	17:45:46.187	-28:59:48.253	11.84	9.91	2023-03-24	840	50/150	5020265	HIP86098
FK87 ⁽¹⁾	17:45:40.671	-29:00:15.318	13.04	10.75	2022-05-16	1620	45/175	87	HIP86098
Feld31 ⁽²⁾	17:45:42.000	-29:00:20.000	13.38	10.61	2023-04-26	1200	20/150	31	HIP86552
Feld84 ⁽²⁾	17:45:39.400	-29:00:58.900	13.90	10.66	2023-04-28	2080	10/135	84	HIP86098
GC15540 ⁽²⁾	17:45:41.900	-28:59:23.390	12.57	10.49	2023-03-24	2200	35/120	3001047	HIP86098
GC16890 ⁽²⁾	17:45:43.900	-28:59:28.500	13.23	10.72	2023-04-26	2240	20/105	3000179	HIP88152
GC13727 ⁽³⁾	17:45:39.590	-28:59:56.210	13.11	10.82	2024-04-11	2520	20/120	73	HIP94663
GC16895 ⁽³⁾	17:45:35.640	-29:00:47.000	13.16	10.75	2024-04-20	2400	20/115	1012095	HIP86098

^aGemini-S Progamme identification: ⁽¹⁾ GS2022A-Q-208; ⁽²⁾ GS2023A-Q-304; ⁽³⁾ GS2024A-Q-304.

^bThe H and K magnitudes are from Nishiyama et al. (2013)

^cThe signal-to-noise ratios were provided by RRISA (The Raw & Reduced IGRINS Spectral Archive; Sawczynec et al. 2022) and are the average S/N for the H- and K-bands per resolution element. The S/N varies over the orders and is lowest at the ends of the orders.

^dIdentification number from Feldmeier-Krause et al. (2017a, 2020).

ing that any possible residuals resulting from the correction process are taken care of.

The spectral orders of the science targets and the telluric standards were subsequently stitched together after normalizing every order and then combining them in *iraf* (Tody 1993), excluding the low S/N edges of every order. This resulted in one normalized stitched spectrum for the entire H and K bands. The spectra were then resampled and to take care of any residual modulations in the continuum levels, we define specific local continua around spectral lines being studied. Finally, the spectra are shifted to laboratory wavelengths in air after a stellar radial velocity correction. We also allowed for small wavelength shifts in the abundance analysis of every spectral line, which allows any errors or trends in the wavelength solution to be taken into account.

Especially toward the Galactic Center, with the large extinction in the line-of-sight, broad absorption features caused by DIBs (diffuse interstellar bands; see, e.g., Geballe 2016) might appear in high-resolution spectra. These are probably due to large molecules in the interstellar medium (ISM). Most DIBs have been identified in optical spectra, but some are found in the NIR (Geballe et al. 2011), and more are being identified with new instruments (e.g., with X-shooter, APOGEE, IGRINS, WINERED, and CRIRES in Cox et al. 2014; Elyajouri et al. 2017; Galazutdinov et al. 2017; Hamano et al. 2022; Ebenbichler et al. 2022, respectively). None of these known DIBs are, however, close to the spectral lines that we use for our abundance determination in this work.

3. ANALYSIS

We determine the abundances of the α -elements Mg, Si, and Ca for 9 M giants in the NSC from their high-resolution spectra and compare the trends of these abundances with those determined for 50 M giants in the solar neighbourhood.

3.1. Nuclear Star Cluster Targets

A detailed abundance analysis of the stellar populations in the NSC requires the use of red giants as probes, observed at high spectral resolution. The significant optical extinction along the line of sight to this region precludes optical analyses. However, reliable abundance determinations can be achieved using high-resolution infrared spectra of K and M giants. In practice, the stars in the NSC that are sufficiently bright for high spectral resolution observations with 10-meter class telescopes are primarily M giants, with effective temperatures below 4000 K. This is attributed to the brightness of these stars, their spectral energy distributions, and the metallicity distribution within the inner regions of the Milky Way. Note that we have deliberately excluded the young M-type supergiants in the NSC from our analysis (such as IRS 7 discussed by Carr et al. 2000; Guerço et al. 2022)². The analysis has been limited to M giants with effective temperatures above 3350 K, for which our analysis method has been tested

²In this study, we differentially determine abundances for low-mass M giants, using a reference sample of the same stellar type. M supergiants, being much more massive, require their own specialized spectroscopic analysis. Our focus here is on M giants, while the young stellar populations in the NSC will offer a complementary perspective to the findings presented in this work (see, e.g., Thorsbro et al. 2023)

Table 2. Stellar and orbit parameters, and C, N, and O abundances for the NSC giants.

Star	T_{eff}	$\log g$	[Fe/H]	ξ_{micro}	[C/Fe]	[N/Fe]	[O/Fe] ^a	μ_l	μ_b	v_{los}	r_{apo}^b	z_{max}
	[K]	[log(cm s ⁻²)]	[dex]	[km s ⁻¹]	[dex]	[dex]	[dex]	[mas/yr]	[mas/yr]	[km s ⁻¹]	[pc]	[pc]
FK48	3440	0.6	0.12	1.8	0.12	0.25	0.09	-2.54	-0.42	0	9.81	6.70
FK5020265	3350	0.6	0.26	1.9	0.06	0.24	0.04	-3.94	5.71	157	9.93	8.47
FK87	3352	0.5	0.09	1.9	0.07	0.35	0.11	–	–	196	–	–
Feld31	3825	1.5	0.42	2.3	-0.04	0.5	-0.04	-1.02	3.25	118	10.32	7.29
Feld84	3709	1.4	0.48	2.7	0.03	0.47	-0.07	–	–	0	–	–
GC15540	3361	0.5	0.11	1.9	0.03	0.36	0.10	-2.68	2.57	0	8.17	6.21
GC16890	3423	0.7	0.19	2.0	0.02	0.33	0.06	-2.07	-1.30	236	8.85	7.02
GC13727	3356	0.4	0.00	2.1	0.20	0.32	0.16	0.74	-0.97	-59	9.17	6.76
GC16895	3366	0.4	-0.12	2.2	0.19	0.45	0.21	-7.93	0.33	-39	11.10	5.03

^aThe [O/Fe] is provided from a simple functional form of the [O/Fe] versus [Fe/H] trend in [Nandakumar et al. \(2023\)](#) based on the [Amarsi et al. \(2019\)](#) trend.

^b r_{apo} is the maximum apocentric radius from the galactic center projected on the x-y plane.

and validated. The targets are given in Table 1 including their coordinates.

In the Table we also provide the star identification from the integral-field, low-resolution ($R = 4, 200$) studies of stars in the NSC of [Feldmeier-Krause et al. \(2017a, 2020\)](#). These authors argued, based on interstellar extinction, that these stars are located in the NSC and are not foreground stars. To further ensure that our stars are bound to the NSC, we also used the dynamical properties of the stars to constrain their membership. The radial velocities are calculated by measuring the wavelength shift of well-identified spectral lines in the observed spectra relative to their corresponding laboratory wavelengths. Proper motions have been obtained for 7 of our targets from the preliminary VIRAC1 ([Smith et al. 2018](#)) photometric and astrometric reduction of the VVV (*VISTA Variables in the Via Láctea*) data ([Minniti et al. 2010](#)). Table 2 gives these proper motions and the line-of-sight velocities. We use the software package AGAMA ([Vasiliev 2019](#)) to determine the orbital parameters by constructing a non-axisymmetric potential by combining the main components of the inner Galaxy that influence the dynamics of the stars: the inner bulge/bar, the NSD, and the NSC. We assume that our stars are located at 8.2 kpc from the Sun. We refer here to [Nieuwmunster et al. \(2024\)](#) for more details. All our targets have typical orbits confined to the NSC and were therefore most-likely formed in-situ.

Figure 2 shows the colour-magnitude diagram of our 9 NSC stars overlaid by the overall population in the NSC. They cover the upper branch of the RGB and a wide (H-K) range.

[Nogueras-Lara et al. \(2021b\)](#); [Nogueras-Lara \(2022\)](#) demonstrated that the membership of stars in the NSC can be determined based on their interstellar reddening. Although interstellar reddening is patchy, they show that in statistical

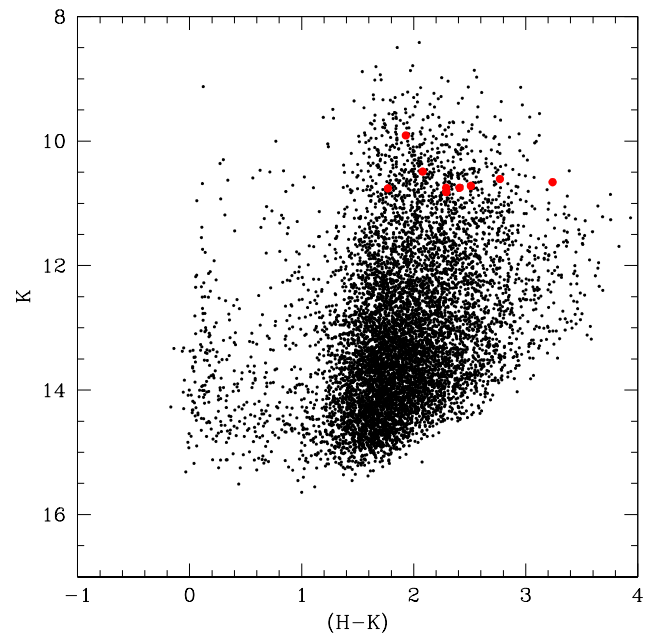


Figure 2. Colour-magnitude diagram, K versus H-K, of the NSC ([Nishiyama et al. 2013](#)) with our observed targets indicated by red circles.

way stars in the NSC do show higher extinction and therefore redder colours in the $J - K$ or $H - K$ diagram. In their Figure 2, they show that stars belonging to the NSC have $H - K$ colours redder than $H - K \sim 1.8$ compared to stars in the NSD or the Galactic bulge. Our sample of stars (see Table 1) have typical colours of $H - K > 1.8$. An additional extinction measurement comes from the diffuse interstellar band (DIB)

clearly visible at $\lambda \sim 1.527 \mu\text{m}$ in our spectra. Although the carrier of the DIBs are still unknown, they correlate well with interstellar reddening (see equation 3 of Zaslowski et al. 2015). A very rough estimate of the equivalent width of the DIB give us typical values in the range of $A_V \sim 20 - 25$, indeed typical for the NSC region.

Together with the above mentioned orbital properties of our stars, we are therefore confident that all our stars belong to the NSC

3.2. Spectroscopic Method

The spectroscopic analysis in this work is done using the spectral synthesis method, where the stellar parameters and elemental abundances of a star are determined by fitting its observed spectrum with a synthetic spectrum. The synthetic spectrum is generated using the Spectroscopy Made Easy (SME) tool (SME; Valenti & Piskunov 1996, 2012), which calculates the spherical radiative transfer through a relevant stellar atmosphere model defined by its fundamental stellar parameters. The stellar atmosphere model is selected by interpolating within a grid of one-dimensional (1D) Model Atmospheres in a Radiative and Convective Scheme (MARCS) stellar atmosphere models (Gustafsson et al. 2008).

The spectral analysis of M giants has received less attention than that of K giants, as K giants are easier to model in the commonly used optical wavelength regions. As a result, the knowledge of line strengths and the identification of suitable lines in infrared spectra of M giants remain limited. To address this, an investigation of the spectra of well-studied stars is necessary to determine the most appropriate spectral lines for analysis. Systematic effects, such as unknown blending lines, can impact certain spectral lines in specific regions of the stellar parameter space. Such investigations were conducted by Nandakumar et al. (2023, 2024a), who provided a recommended set of lines for spectroscopic studies of M giants. We use these recommendations in the following analysis.

3.3. Stellar Parameters

Fundamental stellar parameters - namely, the effective temperature (T_{eff}), surface gravity ($\log g$), metallicity ($[\text{Fe}/\text{H}]$) and microturbulence (ξ_{micro}) - are essential for spectroscopic analysis. These parameters provide the foundation for accurately determining elemental abundances from the respective absorption lines in the observed spectrum. Therefore, it is crucial to determine accurate fundamental stellar parameters. The stellar parameters in this work were determined using the method outlined in Nandakumar et al. (2023) for K and M giants ($T_{\text{eff}} < 4500 \text{ K}$).

3.3.1. Effective Temperature, Metallicity, and Microturbulence

In this method, the effective temperature (T_{eff}) is primarily constrained by selected OH lines sensitive to temperature, while the metallicity is determined using selected Fe lines. Since the OH lines are not only sensitive to the temperature, but also to the oxygen abundance, the main assumption in the method of Nandakumar et al. (2023) is the value of oxygen

abundance. This is taken from a simple functional form of the $[\text{O}/\text{Fe}]$ versus $[\text{Fe}/\text{H}]$ trend in Amarsi et al. (2019) for thick disk stars (see also Figure 1 in Nandakumar et al. (2023) and the study of Rojas-Arriagada et al. (2017)). Thus a weakness of the method is the assumption of the oxygen trend versus metallicity. Typically, a thick- or thin-disk trend is assumed in the method. This assumption is then evaluated against the derived α -abundance trends. A star incorrectly identified as belonging to the thin or thick disk can be detected in this way and a new corrected iteration is performed assuming a correct oxygen trend (for more details, see Nandakumar et al. 2023). A lowering of the assumed oxygen abundance by ~ 0.2 dex for our NSC stars is found to result to systematically lower temperatures of $\sim 50 - 100 \text{ K}$. While this change is within the uncertainties, it is a systematic shift, and leads to an increase of the α -element abundances of 0.05-0.10 dex.

The method presented in Nandakumar et al. (2023) was validated for the temperature range $3400 \lesssim T_{\text{eff}} \lesssim 4000 \text{ K}$, with the lower limit determined by the temperature of the coolest benchmark star used in their study. However, there is no indication that this represents a fundamental limit for the method; it should remain effective at lower temperatures, given the smooth variation of diagnostic lines (OH, CN, CO, and Fe) with decreasing temperature. Our sample includes stars with temperatures approximately 50 K lower, which should not pose any issues for the method. As an initial validation, we do not observe any systematic trends with temperature among our coolest stars. At lower temperatures, water lines become increasingly prominent in the spectra. To accurately model these spectral features, a complete and precise water line list is required. This line list must be thoroughly tested and validated to ensure it provides reliable results, particularly in the cooler atmospheres where water vapor plays a significant role in shaping the observed spectrum.

While the effective temperature and metallicity are mainly constrained in the method by the OH and Fe lines chosen, respectively, selected sets of weak and strong CO and CN lines help constrain the microturbulence (ξ_{micro}). The carbon and nitrogen abundances are simultaneously derived from these CO and CN molecular lines. The lines used are provided in Nandakumar et al. (2023).

3.3.2. Surface Gravity

The surface gravities of the stars were determined using Yonsei-Yale (YY) isochrones, based on the stars' effective temperatures and metallicities (Demarque et al. 2004). The isochrones assume old stellar ages of 2–10 Gyr, which is appropriate for low-mass giants. To investigate the impact of using different sets of isochrones and removing the restriction to old isochrones, we employ the Bayesian isochrone projection code developed by Kordopatis et al. (2023). Originally developed to determine stellar ages, masses and radii, this code also allows for the estimation of the most likely atmospheric stellar parameters based on a set of isochrones. In this case, we will hence compare a set of input parameters (our derived T_{eff} , $\log g$, and $[\text{Fe}/\text{H}]$) by projecting them onto different sets of isochrones. The sets considered are PAR-

SEC (Bressan et al. 2012), MESA (Dotter 2016) and BaSTI (Hidalgo et al. 2018). We ran the code by assuming uncertainties of 100 K, 0.2 dex, 0.1 dex, for T_{eff} , $\log g$ and $[\text{Fe}/\text{H}]$, respectively, and without any prior on age versus metallicity. Isochrones were spaced with a log-age step of 0.05, and a metallicity step of 0.05 dex. The results of the projections are displayed in Figure 3 (orange ‘+’ symbols) for the three sets of isochrones, with PARSEC, MESA (MIST), and BaSTI isochrones presented from top to bottom, respectively. What we find is that the best projection of all isochrone sets yield surface gravities that are close to and consistent with the original ones. This means partly that the exact choice of isochrone-set is not critical, and partly that the assumption of using an old-aged YY isochrone set works well. Isochrones of different ages do, indeed, lie close to each other on the giant branches. Our tests show that the spectroscopic $\log g$ is ~ 0.1 dex larger than the projected values, no matter the isochrones. Implementing the projected $\log g$ as an additional iteration in our stellar parameters determination has a small impact. The T_{eff} of our stars decreases by 0 to 40 K, the metallicities increase by approximately 0.05 dex, and the microturbulence increases by around 0.05 km s^{-1} .

In their analysis of $\log g$ -sensitive line wings in near-infrared spectra, Kocher, J. (2024) demonstrated that for the stars studied in Nandakumar et al. (2023), the surface gravities determined spectroscopically in this way from high S/N spectra are within ± 0.2 dex of those obtained using the isochrone method described in Nandakumar et al. (2023). Additionally, they found that for the same stars, the surface gravities derived from the Bayesian isochrone-fitting tool, PARAM (based on MESA isochrones; da Silva et al. 2006; Rodrigues et al. 2014, 2017), agree within 0.1 dex with those in Nandakumar et al. (2023), assuring that no significant systematic effects are present.

As an additional test of our method for determining surface gravity, we reference the work of Bijavara Seshashayana et al. (2024), who evaluated the performance of the same iterative stellar parameter determination method ($\log g$, from YY-isochrones) used in this study by applying it to six field M giant stars from the *Kepler* database. They determined the stellar parameters for these stars from their high resolution ($R \sim 50,000$) GIANO-B spectra and then compared the resulting $\log g$ values with the asteroseismic $\log g$ -values in the APOGEE and Kepler Asteroseismology Science Consortium (APOKASC-3) catalog. They find overall good agreement for all six stars with a minimum difference of $+0.01$ dex and a maximum difference of $+0.18$ dex between the isochrone-derived and asteroseismic $\log g$ values (see their Table 4 for more details). These differences are consistent with the estimated uncertainty of ± 0.2 dex in $\log g$ from this method.

3.4. Spectral Lines and Stellar Abundances

For the determination of the stellar abundances of Mg, Si, and Ca, we thus base our line list on the studies by Nandakumar et al. (2023, 2024a). We have also added two additional silicon lines in the K band ($\lambda_{\text{air}} = 21368.7$ and 21874.2 \AA). In our analysis, we incorporate departure coeffi-

cients from non-local thermodynamic equilibrium (non-LTE) grids for the elements C, N, O, Mg, Si, Ca, and Fe (Amarsi et al. 2020, 2022). The line data for the CO, CN, OH, and H₂O lines were adopted from the line lists of Li et al. (2015), Brooke et al. (2016), Sneden et al. (2014), and Polyansky et al. (2018), respectively. The molecular lines are important since they might blend with and affect the abundance determination from many of the atomic spectral lines. We have scaled the finally derived abundances with respect to the solar abundance values from Grevesse et al. (2007).

3.5. Reference Sample

Nandakumar et al. (2023, 2024a) also provide a detailed abundance analysis of a comparison sample of 50 M giants in the solar neighborhood, observed using the same observational setup and analyzed with the same method, including the same stellar parameter scale and spectral lines, as employed in our study presented here. The primary advantage is the ability to directly and differentially compare our findings for the NSC stars with the abundance trends for the solar neighborhood sample, element by element and line by line. This approach minimizes systematic uncertainties, with the only difference between the analysis of the NSC sample and the solar neighborhood sample being the slightly lower S/N of the former. In the following sections, we adopt the terminology from Haywood et al. (2013); Di Matteo (2016) by referring to the inner-disk sequence, when mentioning the thick disk and metal-rich thin disk (see Section 5).

4. RESULTS

The effective temperatures for our NSC stars range from 3350 and 3850 K, while those of the solar neighbourhood sample fall within the range of $3400 \lesssim T_{\text{eff}} \lesssim 4000$ K. The surface gravities, $\log g$, lie between 0.3 and 1.5 and the metallicities between $-0.1 \lesssim [\text{Fe}/\text{H}] \lesssim 0.5$. Table 2 provides the final stellar parameters of the NSC stars, as well as their $[\text{C}/\text{Fe}]$, $[\text{N}/\text{Fe}]$, and assumed $[\text{O}/\text{Fe}]$ abundances.

4.1. α -Element Trends

Our results for the abundance trends of the α elements as a function of metallicity are presented in Figures 4 to 6, with each figure corresponding to a different element. The trends for the stars in the NSC (black star symbols) are compared with those observed in the solar neighbourhood including low- α or thin-disk stars (in red circles) and high- α or thick-disk stars (in orange diamonds). Additionally, the trends determined by Nandakumar et al. (2024b) for inner-bulge stars located 1 degree North of the Galactic Center are indicated by blue squares. These inner-bulge stars display a trend following the inner-disk sequence, aligning with the high- $[\alpha/\text{Fe}]$ envelope of the metal-rich, thin-disk population in the solar vicinity, but having the same α -enhancements as the solar vicinity thick-disk stars of the same $[\text{Fe}/\text{H}]$ (cf. Haywood et al. 2013).

In the Figures, we display both the final mean trends and the trends derived on a line-by-line basis. This approach allows us to examine any systematic effects that may arise

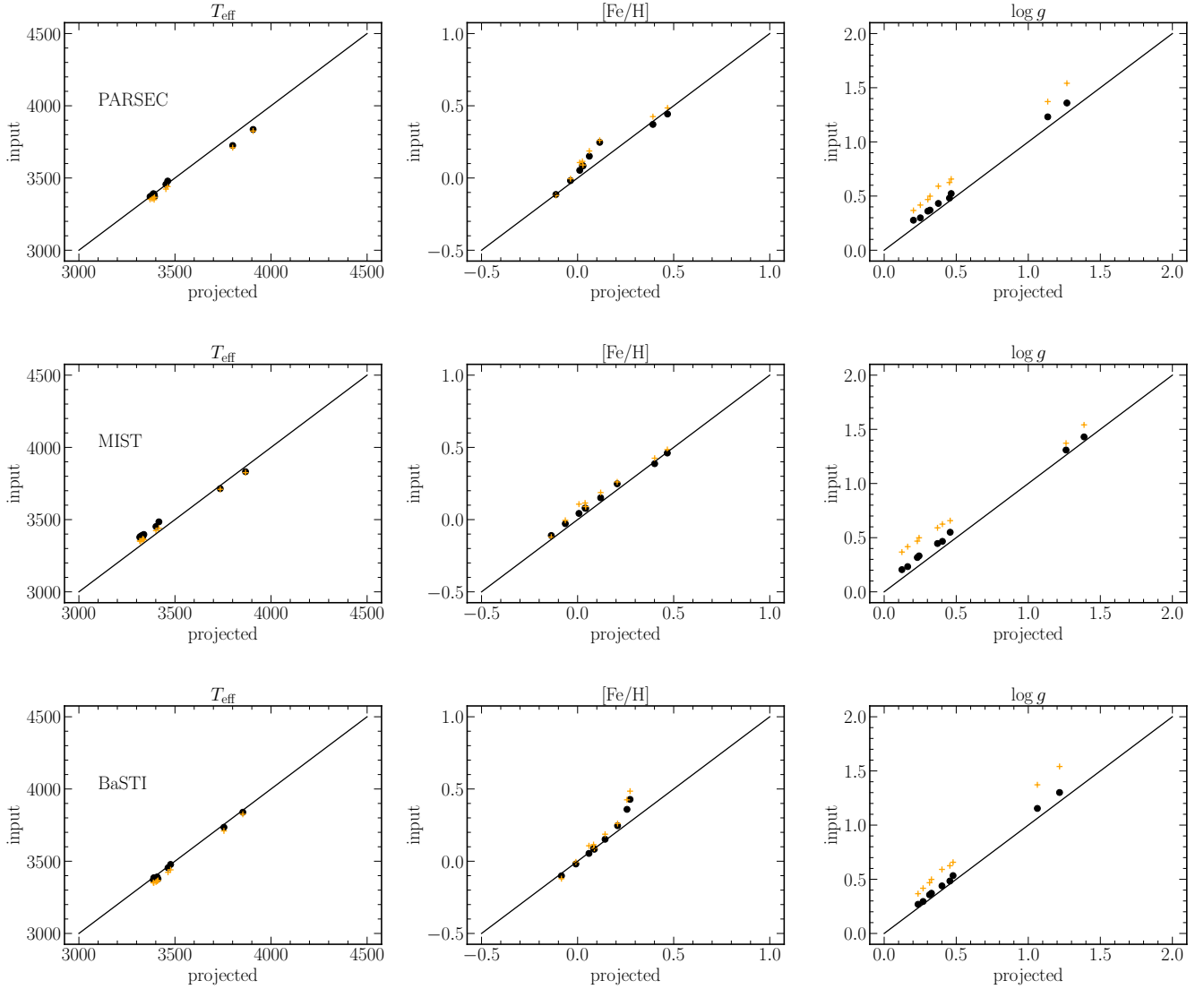


Figure 3. Input parameters versus isochrone-projected ones, for T_{eff} (first column), $[\text{Fe}/\text{H}]$ (second column) and $\log g$ (third column) using the [Kordopatis et al. \(2023\)](#) code. First row shows the projection on PARSEC isochrones, second on MIST, and third on BaSTI (solar scaled). Points far from the diagonal indicate that no isochrones are found close to the input values. Yellow ‘+’ signs are the atmospheric parameters from the first iteration ($\log g$ obtained from the YY isochrones), whereas the black points are the results for a second (and final) projection, once new spectroscopic T_{eff} and metallicities are determined taking into account the projected $\log g$ from the first iteration. One can notice that a very good convergence is reached in that case.

for different spectral lines. The spectral lines used are based on the recommendations by [Nandakumar et al. \(2023\)](#), who identify lines that yield reliable results for high-quality spectra of M giants in the solar neighbourhood. For magnesium (Mg) and silicon (Si), three and five K-band lines were used, respectively. For calcium (Ca), three H-band lines were used. The line wavelengths are also given in the Figures 4-6.

The systematic uncertainties are difficult to quantify; however, our differential analysis ensures that these uncertainties impact both samples in a similar way. The main random uncertainty in the determined elemental abundance ratios are due to the uncertainties in the stellar parameter determina-

tion. We follow the determination of the uncertainties in the abundances as outlined in [Nandakumar et al. \(2024a\)](#) and [Nandakumar et al. \(2024b\)](#) for the solar neighbourhood stars and the stars at $(l, b) = (0^\circ, +1^\circ)$, respectively. In summary, we recalculated 50 abundance values for different sets of stellar parameters, randomly selected from normal distributions with standard deviations representing typical uncertainties (± 100 K in T_{eff} , ± 0.2 dex in $\log g$, ± 0.1 dex in $[\text{Fe}/\text{H}]$, and ± 0.1 km s $^{-1}$ in ξ_{micro}). The abundance uncertainties range from 0.05 to 0.15, and are shown as error bars in the trend Figures 4 - 6.

In the Figures 4 to 6, we also provide examples of typical line appearances from high S/N spectra of M giants in the solar neighborhood, as well as the line appearances from the typical NSC star FK48 ($T_{\text{eff}} = 3440$ K, $\log g = 0.6$, $[\text{Fe}/\text{H}] = +0.12$, see Table 2). These serve to illustrate typical line strengths that were used in the abundance analysis, as we aim to avoid lines that are too weak, which may disappear in the noise, as well as lines that are too strong, which may be significantly affected by the uncertain value of the microturbulence or formed in the outer, tenuous regions of the stellar atmosphere where the structure is not well modeled.

4.2. Individual α -Element Trends

Overall, we observe clear enhancements in the α -element abundances for the NSC stars, consistent with the trend found for stars located 1 degree North of the Galactic Center, which we will refer to as 'inner-bulge stars' in the following. Below, we examine the individual α -element trends in detail.

Magnesium. The $[\text{Mg}/\text{Fe}]$ -trend follows the inner-bulge trend within uncertainties, as shown in Figure 4. It is clearly following the upper envelope of the metal-rich part of the thin-disk stars (red). The $[\text{Mg}/\text{Fe}]$ ratios of the two metal-rich stars at $[\text{Fe}/\text{H}] \gtrsim 0.4$ are clearly subsolar, extending a downward trend.

Silicon. Similarly, the $[\text{Si}/\text{Fe}]$ -trend also follows that of the inner-bulge stars, see Figure 5. The trend exhibits less scatter, which can be attributed to the use of five different spectral lines, all of which display quite a small scatter. The most metal-rich stars also show subsolar $[\text{Si}/\text{Fe}]$ ratios.

Calcium. The mean $[\text{Ca}/\text{Fe}]$ -trend is derived from three spectral lines, lying in quite blended regions in the H band, see Figure 6. The surrounding spectra are, however, well modelled and continuum regions can be defined nearby, which gives us confidence in the accuracy of the derived Ca abundances. While some variations are observed among the trends of the individual lines, there is a clear decreasing trend in the $[\text{Ca}/\text{Fe}]$ ratio with increasing metallicity, following the upper envelope of the thin-disk stars.

The H-band lines are expected to have a lower S/N than several potentially useful K-band lines. The K-band lines are beautiful, strong, and seemingly unblended. However, the abundances derived from them show a larger scatter in all data sets, with some abundance values systematically and significantly higher than expected from the H-band lines. This discrepancy between H-band and K-band lines, increasing with metallicity, was also addressed by Lim et al. (2022) in their near-IR spectroscopic study observing K giants toward the bulge with the IGRINS spectrometer. They identified such a discrepancy for Ca, Al, and Ti but not for all elements in their study. They explored potential causes for this difference, such as uncertainties in line strengths, difficulties in continuum definition, or the effects of non-LTE, but did not identify a definitive cause for the discrepancy. Until these differences in abundances are understood, especially for high metallicities, we choose to only use the H-band lines of calcium. Thus, our final mean Ca trend shows a decreasing trend with metallicity, similar to the inner-bulge stars,

with the two most metal-rich stars showing subsolar $[\text{Ca}/\text{Fe}]$ ratios.

Mean α -abundance trend. In the left panel of Figure 7, we have combined the trends into a single, general α -abundance trend, despite recognizing that the different α elements should exhibit slightly different trends (see, e.g., Woosley & Weaver 1995; Matteucci 2021). The NSC $[\alpha/\text{Fe}]$ trend shows a clear and steady decrease with increasing metallicity, with the two most metal-rich stars displaying subsolar ratios. In order to approximately quantify the difference in trends between the different stellar populations, we carried out a simple polynomial fit to the mean α -abundance trends and estimated the standard deviations. In the right panel of Figure 7, we show the fit and the standard deviations with solid lines and similar colored bands respectively. For the solar neighbourhood trend we show the running mean instead. For the NSC population, we do not include the two most metal rich stars since there are no similar metallicity stars in the solar neighborhood population. The trends of the inner-bulge and NSC stellar populations are clearly similar and overlap with each other. Hence we cannot reject the hypothesis that they are drawn from a similar population. The mean trends of the NSC and that of the inner-bulge lie slightly higher than that of the solar neighborhood metal-rich, thin-disk stars by approximately 0.1 dex in abundance, which slightly exceeds 1σ of the NSC population. The NSC and inner-bulge trends, however, follow the upper envelope of the thin-disk stars, consistent with the inner-disk sequence distribution.

5. DISCUSSION

A detailed chemical characterization of the stellar populations in the Galactic Center region is essential for unraveling its formation history and understanding the relationships between the different structures located within it. Here, we will compare the diagnostically interesting α -element trends in the NSC directly with a comparison set observed in the solar neighbourhood. We will also conduct a differential and direct comparison with the inner-bulge population located at 1° North of the Galactic Center, as investigated by Nandakumar et al. (2024b), using the same methodology applied in this study.

The trend of the $[\alpha/\text{Fe}]$ abundance ratio versus the metallicity, $[\text{Fe}/\text{H}]$, of a stellar population, is useful for determining the star-formation history of that population (see, for instance, McWilliam 1997; Matteucci 2021). The reason is that the $[\alpha/\text{Fe}]$ abundance ratio found in stars depend partly on the α abundances in the star-forming cloud, abundances that is formed on short time-scales from massive stars (expelled during the core-collapse supernova (CCSNe) explosion), and partly on the iron abundance, which is formed on longer time-scales in thermonuclear supernovae (SN Type Ia, SN Ia). The star-formation rate will determine the increase of the metallicity with time. Magnesium is predominantly produced during the hydrostatic burning stage over a massive stars's lifetime. Si and Ca are mainly explosive α -elements and are produced in the CCSNe explosion (see, e.g., Woosley

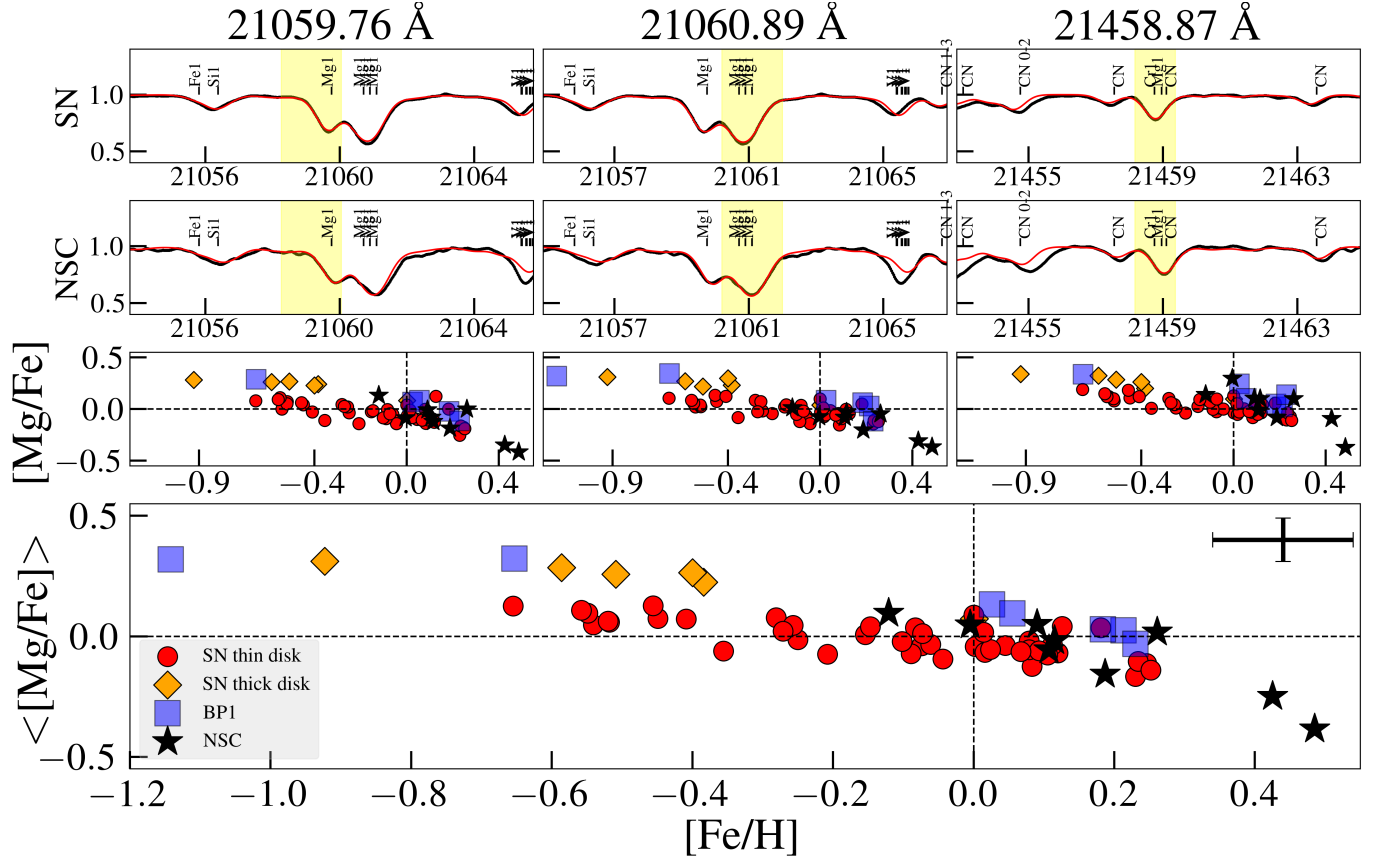


Figure 4. $[\text{Mg}/\text{Fe}]$ versus $[\text{Fe}/\text{H}]$ for different stellar populations. The Nuclear Star Cluster (NSC) stars are represented by black stars, the inner bulge stars from Nandakumar et al. (2024b) by blue squares, and the solar neighborhood thin-disk stars are depicted by red filled circles, while the thick-disk stars are shown as orange diamonds. In the upper two panels, the spectral lines used for the analysis are displayed, with a typical solar neighborhood star shown above and a typical NSC star (FK48) shown below. The trends derived from each individual spectral line are presented, along with the mean trend, which is displayed in the largest, bottom panel.

& Weaver 1995; Matteucci 2021). Whereas magnesium is nearly solely formed in massive stars, it should be noted that, for instance, silicon is produced both in CCSNe and in SN Ia in almost equal proportions (Matteucci et al. 2020).

Any differences in α -element trends between populations would reveal environmental influences on, for example, the star-formation histories and processes, gas-flow patterns, evolutionary timescales, and stellar evolutionary processes in the different populations (see, for instance, Friske & Schönrich 2023). The α -element trends and their scatter are also useful for determining the spatial (e.g. in situ or accreted) and temporal origins of the stars in that population (see, for example, Agertz et al. 2021; Renaud et al. 2021b), as well as properties of the interstellar medium, e.g. the gas depletion time in star forming clouds (see e.g. figure 9 in Renaud et al. 2021a).

As a background, the established α -abundance trends of the bulge/bar appear similar to a thick disk extending to higher metallicities (Meléndez et al. 2008; Ryde et al. 2010; Kordopatis et al. 2015; Rojas-Arriagada et al. 2017; Zsawski et al. 2019; Lomaeva et al. 2019; Nieuwmunster et al. 2023). This can be compared to the picture suggested in Di

Matteo (2016) where the thick-disk (high α) stellar population in the solar neighbourhood is referred to as the ‘inner disk sequence’; the metal-rich, thin-disk population that is joined by the ‘inner-disk sequence’ is referred to as the ‘inner thin disk’ and it is considered to be the same structure as the thick-disk or ‘inner-disk sequence’ (see also Haywood et al. 2013). A comparable scenario is observed in the cosmological zoom-simulation VINTERGATAN (Ageritz et al. 2021; Renaud et al. 2021a) of a Milky Way-like galaxy, where the chemically-defined thin disk stars in the solar neighborhood are shown to have formed in an outer disk. Furthermore, a general view is emerging according to which the dynamical bar becomes dominant for $[\text{Fe}/\text{H}] > -0.5$ dex (Soto et al. 2007; Ness et al. 2013), with the metal-rich stars more concentrated to the Galactic plane (Johnson et al. 2020, 2022). This metal-rich structure of the bulge is most likely of a secular formation origin from the early disk (Shen et al. 2010; Ness et al. 2012; Rojas-Arriagada et al. 2017, 2020; Zoccali et al. 2017). The investigation by Nandakumar et al. (2024b) of the inner-bulge population located at 1° N showed a similarity between the inner-bulge population and the inner-disk

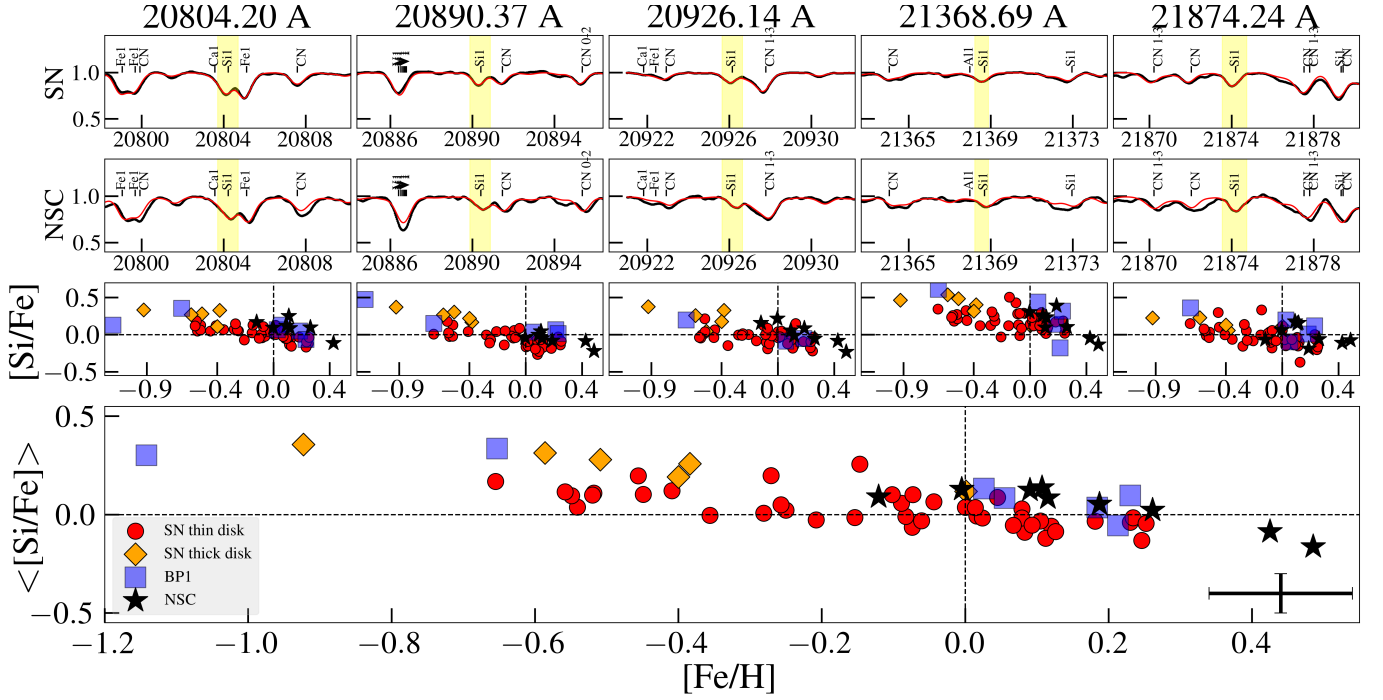


Figure 5. $[\text{Si}/\text{Fe}]$ versus $[\text{Fe}/\text{H}]$ for different stellar populations: NSC stars (black stars), inner bulge stars (blue squares), thin-disk stars (red circles), and thick-disk stars (orange diamonds). The upper panels display the spectral lines used, with a typical solar neighborhood star above and an NSC star (FK48) below. Trends from individual lines and the mean trend are shown in the bottom panel.

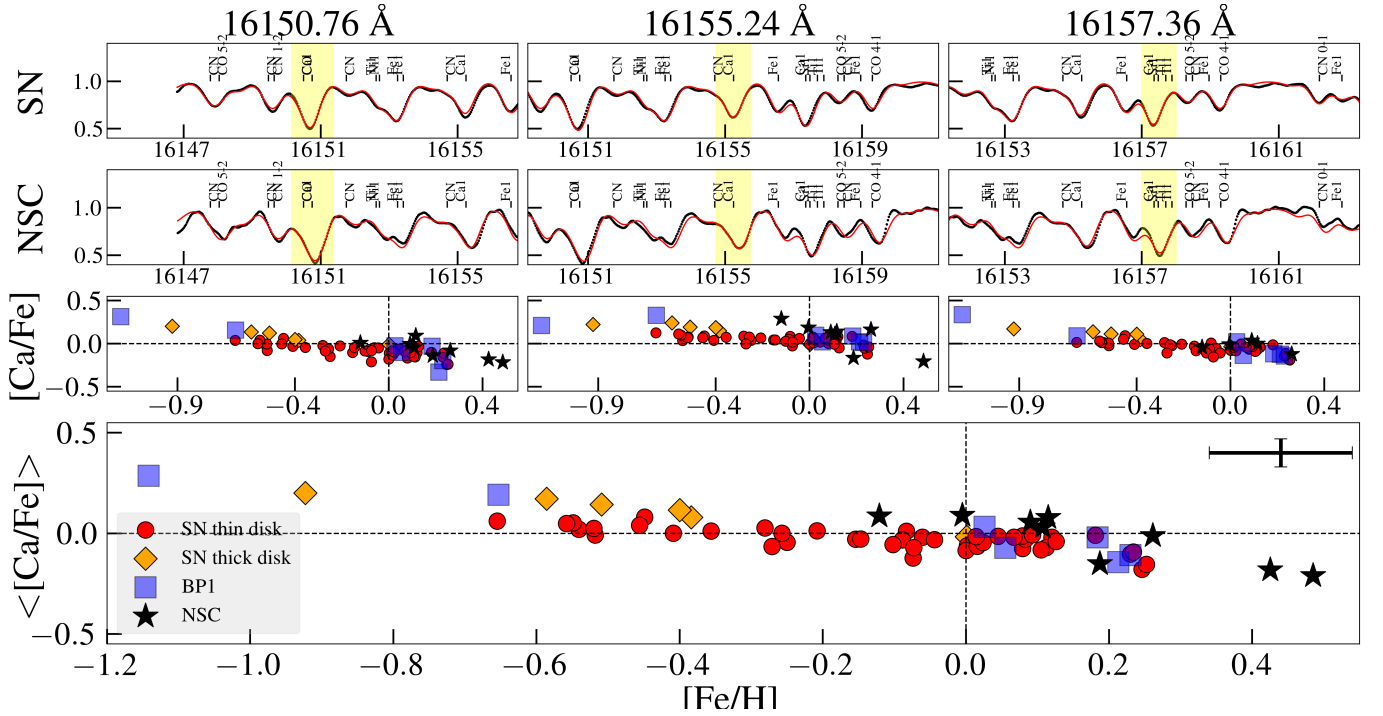


Figure 6. $[\text{Ca}/\text{Fe}]$ versus $[\text{Fe}/\text{H}]$ for different stellar populations: NSC stars (black stars), inner bulge stars (blue squares), thin-disk stars (red circles), and thick-disk stars (orange diamonds). The upper panels display the spectral lines used, with a typical solar neighborhood star above and an NSC star (FK48) below. Trends from individual three lines and the mean $[\text{Ca}/\text{Fe}]$ trend versus metallicity are shown in the bottom panels.

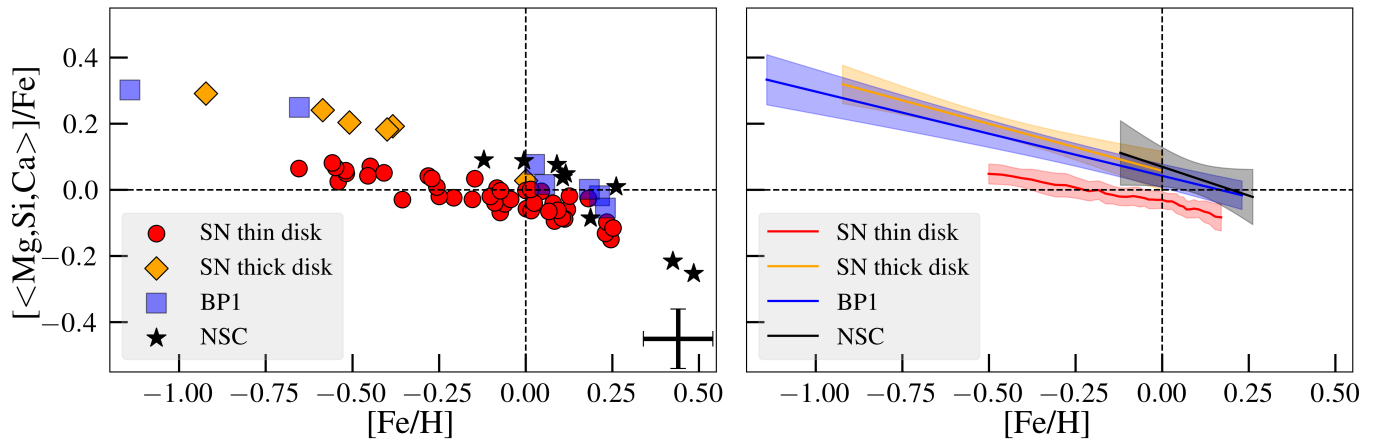


Figure 7. Straight mean abundance of the three α elements, Mg, Si, and Ca versus $[\text{Fe}/\text{H}]$ for the NSC (black), inner-bulge stars located 1 degree North of the Galactic Center (blue), thick-disk (orange), and thin-disk stars (red). Left panel: Scatter plot of the mean α abundances. Right panel: Running mean for the solar neighbourhood trend and simple polynomial fits (solid line) to the mean α abundances and the respective standard deviations (respective colored band). This shows a slight difference ($\sim 1\text{-}\sigma$) between the trends of the solar neighbourhood and NSC populations (also thick disk and inner bulge). We excluded the two most metal rich stars in the NSC for the fit since there are no similar metallicity stars in the solar neighborhood stellar population.

sequence, following the high- $[\alpha/\text{Fe}]$ envelope of the solar vicinity metal-rich, thin-disk population.

While the majority of stars in the Galactic Center are generally very old (> 8 Gyr), with those in the NSC being more than 10 Gyr old (Schödel et al. 2020), steady gas inflows channeled by the Galactic bar have indeed triggered bursts of younger star formation over time. It is believed that as much as 15% of the total star formation gave rise to an intermediate-aged (~ 3 Gyr) population in the NSC (Nogueras-Lara et al. 2021a). In contrast, Chen et al. (2023) do not identify the old population, but a dominant, metal-rich component (constituting over 90% of the stellar mass) with an age of around 5 Gyrs. The star formation history of the bulge as a whole is also found to be complex with a range of ages found for metal rich stars ($[\text{Fe}/\text{H}] > 0$). For instance, Bensby et al. (2017) estimated 35% of metal rich stars to be younger than 8 Gyr while Joyce et al. (2023) estimated it to be only 18% by reassessing the ages of a subset of the same stars with a different isochrone set.

Our α -element trends as a function of metallicity in the NSC all decrease with increasing metallicity also at the highest metallicities, which is expected from Galactic Chemical Evolution models (see, e.g., Grisoni et al. 2017; Matteucci 2021). We also observe that the trends for Mg, Si, and Ca (as well as the mean α -element trend shown in Figure 7) show similarities to those observed in the inner bulge located at $(l, b) = (0, +1^\circ)$ (Nandakumar et al. 2024b). These trends also align with the broader characteristics of the bar population and the inner-disk sequence, following the high- $[\alpha/\text{Fe}]$ envelope of the metal-rich population in the solar vicinity. This suggests that the chemical pattern observed in the NSC stars is consistent with that seen in solar vicinity thick-disk stars at the same $[\text{Fe}/\text{H}]$ values, exhibiting similar levels of α -element enhancement. This is interesting because the thick-disk sequence, extending to its metal-rich limit, appears to be the only chemical sequence in both the inner disk and the Bulge (the so-called inner-disk sequence). Thus, our NSC stars appear to be located on top of the chemical sequence found in the inner Galaxy, on much larger spatial scales.

Since the α -elements versus $[\text{Fe}/\text{H}]$ patterns are so similar, this suggests that the star-formation history (SFH) of the NSC (at these metallicities) and of the thick disk, at the same metallicities, must also have been similar. Because of the existence of a strong link between the SFH of the thick disk and the Bulge (see, e.g., Haywood et al. 2018), this suggests a surprisingly similar evolution of the star formation from a several-kpc scale (the thick disk), to a few-kpc scale (the Bulge) up to the innermost central regions of the Milky Way (the NSC).

Thus, the similarities suggest that the NSC may resemble the inner bulge, which in Matteucci et al. (2019) is described as being *predominantly* old with a rapid star-formation history. This would allow us to rule out a dominant 5 Gyr starburst in favour of an 8–10 Gyr burst. In fact, in Nieuwmunster et al. (2023), a chemical evolution model was proposed to reproduce the α -element abundance trends in the inner-bulge within $|b| < 2^\circ$, showing peaks in the star-formation

rate concentrated to the first 4 Gyr of the evolution of the bulge (i.e. ages older than ~ 10 Gyr). It is not necessarily possible, however, to completely rule out the presence of a 3 Gyr-old burst responsible for the formation of an intermediate-aged population in the NSC (Schödel et al. 2020; Nogueras-Lara et al. 2021a). If such a burst accounts for a relatively small fraction of the total star-formation rate, it may only cause a minor change in the observed α -element abundance pattern. This effect could be obscured by uncertainties, and can only be conclusively ruled out through a detailed chemical evolution model, which will be the focus of future investigations. Investigating the influence and magnitude of early gas inflows into the NSC region on the observed α -element trends in this study would also be highly valuable. However, we emphasize that our sample size is small, limiting the constraints we can place on the star-formation history of the NSC. The upcoming MOONS survey (Gonzalez et al. 2020) will significantly increase the sample size in the NSC, helping to provide a more comprehensive understanding of the complex star-formation history in this region.

The detailed spectroscopic analysis of more than 1000 FGK dwarf stars in the solar neighborhood using the high-resolution ($R \sim 115\,000$) spectra from the HARPS-GTO program have revealed a population of high α metal rich ($h\alpha mr$) stars (Adibekyan et al. 2011; Delgado Mena et al. 2019). The $h\alpha mr$ population have $[\text{Fe}/\text{H}] > -0.2$ dex, enhanced $[\alpha/\text{Fe}]$ ratios with respect to the thin disk stars and are found to be older (> 6 Gyr) than the thin disk stars at similar metallicities (see Fig. 5 in Delgado Mena et al. 2019). A link between the $h\alpha mr$ stars and stars in the inner Galactic disk or the bulge have been proposed by Adibekyan et al. (2011). We do not find similar stars in our solar neighborhood sample since they are rare and hence difficult to find among such small sample of stars. We, therefore, note that the absence of the $h\alpha mr$ stars in our reference sample further accentuates the enhancement in alpha abundances for the NSC and inner bulge populations compared to the metal rich thin disk stars. Hence we reassert that our NSC and inner-bulge stars follow the high α envelope of the solar vicinity metal-rich population.

Although our sample size is small and we have not accounted for potential selection effects, the metallicity distribution of the NSC stars analyzed in this study corroborates the broad abundance range reported in the first paper of this series (Rich et al. 2017). Specifically, we confirm the presence of stars with metallicities up to $[\text{Fe}/\text{H}] = +0.5$. We note that we find few stars with subsolar metallicities in our sample, but red giants with lower metallicities tend to be warmer, and we have intentionally excluded these stars from our analysis due to spectroscopic constraints. The distribution of metallicities as a function of latitude and longitude is otherwise a strong diagnostics and could be compared to that of the local thick disk and with model prediction of the modulation of the metallicity distribution function (MDF) with latitude and longitude, as observed over the whole bulge extent (see, for e.g., Fragkoudi et al. 2018).

At supersolar metallicities, we observe a clear decreasing trend in α -element abundances; however, we do not detect the elevated [Si/Fe] values reported in the second paper of this series by Thorsbro et al. (2020). It is possible that these high- α stars belong to a distinct population within the NSC. Thorsbro et al. (2020) acknowledged that their conclusions were based on a small sample size and highlighted the need to verify the trend using other α -elements. Unfortunately, we lack IGRINS spectra for the stars analyzed in that study, which would not only have provided us with the [Mg/Fe] and [Ca/Fe] trends versus [Fe/H], but also have enabled a differential analysis. Such an analysis would clarify the influence of analysis differences due to the lower resolution, limited K-band coverage, application of non-LTE corrections, or possible differing temperature scales, or the cooler temperatures of the stars in Thorsbro et al. (2020) (3300–3450 K) compared to our metal-rich stars (3700–3800 K). It cannot be excluded that there might be a complex high-metallicity environment with a spread in [Si/Fe] values. Thorsbro et al. (2023) further suggest a complex chemical evolution and enrichment in the NSC by finding a wide metallicity range of 1.7 dex among three \sim 3-Gyr-old NSC stars. A systematic survey of a larger sample of NSC stars, which will be provided by the MOONS survey, is necessary to identify and evaluate potential substructures within the NSC.

6. CONCLUSIONS

This study is part of a series characterizing the chemical evolution of the Nuclear Star Cluster (NSC) of the Milky Way and its relation to the Galactic inner regions, with implications for understanding the formation history and evolution of the Milky Way’s central stellar populations. A detailed chemical abundances analysis is needed for such studies. However, the Galactic Center has been largely unexplored chemically due to significant optical extinction along the line-of-sight. High-quality, high-resolution, near-infrared spectroscopic data are necessary to achieve the precision and accuracy required for such analysis. The IGRINS spectrometer mounted on a 10-meter class telescope, fulfills these criteria, covering the full H and K bands in its observations.

Comparing the chemical histories of different stellar populations is a powerful tool. The abundance trends of the α elements are a key diagnostic, offering insights into the star-formation rate and in-fall history. In this study, we have, therefore, determined detailed abundances and their trends with metallicity for the α -elements Mg, Si, and Ca in 9 M-giants in the NSC, observed using IGRINS on the Gemini South telescope. We performed a robust membership analysis of the target stars to ensure that they are indeed NSC stars. These results are compared to derived abundances of M giants in the solar neighborhood and of a sample of M-giants located 1° North of the Galactic Center (i.e. beyond the NSD) presented in Nandakumar et al. (2024b). To ensure a strictly differential analysis and minimize systematic uncertainties, we employed the same instrument, wavelength range, spectral resolution, reduction pipelines, and analysis techniques for determining the stellar parameters and ele-

mental abundances across all samples. All stars are of similar type and span the same parameter space in terms of fundamental stellar parameters.

We find enhanced [α /Fe] ratios for the predominantly metal-rich stars in the NSC. We see similar trends for all of the investigated α elements, namely Mg, Si, and Ca. These α -element trends closely align with those in the inner bulge located at $+1^\circ$ N derived by Nandakumar et al. (2024b), following the upper envelope of the metal-rich, thin-disk stars in the solar neighborhood, and following the inner-disk sequence. This pattern suggests a higher star-formation rate in the inner regions compared to that of the solar neighborhood. Our findings suggest that the NSC population likely shares a similar evolutionary history with the inner-bulge population. Given that the inner-bulge population is presumed to have formed through a rapid and early star-formation history (Matteucci et al. 2019), our data do not rule out the 10 Gyr-old star formation dominance in the NSC described by Schödel et al. (2020), but would not fit with the scenario of a more recent, dominant burst of star formation proposed by Chen et al. (2023). Detailed Galactic Chemical Evolution models are, however, needed to test the effects on the α -element enhancements of different star-formation histories. The similarity also points to an in-situ formation of, at least, the metal-rich population in the NSC of the Milky Way (Neumayer et al. 2020).

In a forthcoming paper, we will explore abundance trends for additional classes of elements, similar to the analysis of inner-bulge stars by Nandakumar et al. (2024b), and examine their respective evolutionary timescales. The nucleosynthetic channels traced by these elements will offer further insight into the relationship between the NSC and the inner-disk sequence of the Milky Way. If this connection is confirmed, it would suggest that the chemical properties of extragalactic NSCs in galaxies of a mass like the Milky Way could serve as valuable proxies for understanding the evolutionary processes of their host galaxies, in a manner explored first by Pagnini et al. (2024).

Further investigations of chemical abundances in the young population should be conducted, as they would provide insights into the recent chemical evolution. This approach was pioneered by Cunha et al. (2007), who demonstrated elevated α -element abundances at high metallicities.

Acknowledgements

We would like to thank Bengt Edvarsson, Thomas Masseron, and Henrik Jönsson for help with the EXOMOL water list of Polyansky et al. (2018). N.R. acknowledge support from the Swedish Research Council (grant 2023-04744) and the Royal Physiographic Society in Lund through the Stiftelsen Walter Gyllenbergs, Märta och Erik Holmbergs, and Henry och Gerda Dunkers donations. G.N. acknowledges the support from the Wenner-Gren Foundations (UPD2020-0191 and UPD2022-0059) and the Royal Physiographic Society in Lund through the Stiftelsen Walter Gyllenbergs fond. G.N. also acknowledges the support received from the Royal Swedish Academy of Sciences (Vetenskapsakademiens stif-

telser). O.A. acknowledges support from the Knut and Alice Wallenberg Foundation, the Swedish Research Council (grant 2019-04659), and the Swedish National Space Agency (SNSA Dnr 2023-00164). B.T. acknowledges the financial support from the Wenner-Gren Foundation (WGF2022-0041). A.M.A. acknowledges support from the Swedish Research Council (VR 2020-03940) and from the Crafoord Foundation via the Royal Swedish Academy of Sciences (CR 2024-0015). This work used The Immersion Grating Infrared Spectrometer (IGRINS) was developed under a collaboration between the University of Texas at Austin and the Korea Astronomy and Space Science Institute (KASI) with the financial support of the US National Science Foundation under grants AST-1229522, AST-1702267 and AST-1908892, McDonald Observatory of the University of Texas at Austin, the Korean GMT Project of KASI, the Mt. Cuba Astronomical Foundation and Gemini Observatory. This work

is based on observations obtained at the international Gemini Observatory, a program of NSF's NOIRLab, which is managed by the Association of Universities for Research in Astronomy (AURA) under a cooperative agreement with the National Science Foundation on behalf of the Gemini Observatory partnership: the National Science Foundation (United States), National Research Council (Canada), Agencia Nacional de Investigación y Desarrollo (Chile), Ministerio de Ciencia, Tecnología e Innovación (Argentina), Ministério da Ciência, Tecnologia, Inovações e Comunicações (Brazil), and Korea Astronomy and Space Science Institute (Republic of Korea). The following software and programming languages made this research possible: TOPCAT (version 4.6; Taylor 2005); Python (version 3.8) and its packages ASTROPY (version 5.0; Astropy Collaboration et al. 2022), SCIPY (Virtanen et al. 2020), MATPLOTLIB (Hunter 2007) and NUMPY (van der Walt et al. 2011).

REFERENCES

- Adibekyan, V. Z., Santos, N. C., Sousa, S. G., & Israelian, G. 2011, *A&A*, 535, L11, doi: [10.1051/0004-6361/201118240](https://doi.org/10.1051/0004-6361/201118240)
- Agertz, O., Renaud, F., Feltzing, S., et al. 2021, *MNRAS*, 503, 5826, doi: [10.1093/mnras/stab322](https://doi.org/10.1093/mnras/stab322)
- Amarsi, A. M., Liljegren, S., & Nissen, P. E. 2022, *A&A*, 668, A68, doi: [10.1051/0004-6361/202244542](https://doi.org/10.1051/0004-6361/202244542)
- Amarsi, A. M., Nissen, P. E., & Skúladóttir, Á. 2019, *A&A*, 630, A104, doi: [10.1051/0004-6361/201936265](https://doi.org/10.1051/0004-6361/201936265)
- Amarsi, A. M., Lind, K., Osorio, Y., et al. 2020, *A&A*, 642, A62, doi: [10.1051/0004-6361/202038650](https://doi.org/10.1051/0004-6361/202038650)
- Arca-Sedda, M., & Capuzzo-Dolcetta, R. 2014, *MNRAS*, 444, 3738, doi: [10.1093/mnras/stu1683](https://doi.org/10.1093/mnras/stu1683)
- Astropy Collaboration, Price-Whelan, A. M., Lim, P. L., et al. 2022, *ApJ*, 935, 167, doi: [10.3847/1538-4357/ac7c74](https://doi.org/10.3847/1538-4357/ac7c74)
- Baba, J., & Kawata, D. 2020, *MNRAS*, 492, 4500, doi: [10.1093/mnras/staa140](https://doi.org/10.1093/mnras/staa140)
- Bensby, T., Feltzing, S., Gould, A., et al. 2017, *A&A*, 605, A89, doi: [10.1051/0004-6361/201730560](https://doi.org/10.1051/0004-6361/201730560)
- Bijavara Seshashayana, S., Jönsson, H., D'Orazi, V., et al. 2024, *A&A*, 689, A120, doi: [10.1051/0004-6361/202451056](https://doi.org/10.1051/0004-6361/202451056)
- Bland-Hawthorn, J., & Gerhard, O. 2016, *ARA&A*, 54, 529, doi: [10.1146/annurev-astro-081915-023441](https://doi.org/10.1146/annurev-astro-081915-023441)
- Bressan, A., Marigo, P., Girardi, L., et al. 2012, *MNRAS*, 427, 127, doi: [10.1111/j.1365-2966.2012.21948.x](https://doi.org/10.1111/j.1365-2966.2012.21948.x)
- Brooke, J. S. A., Bernath, P. F., Western, C. M., et al. 2016, *JQSRT*, 168, 142, doi: [10.1016/j.jqsrt.2015.07.021](https://doi.org/10.1016/j.jqsrt.2015.07.021)
- Capuzzo-Dolcetta, R. 1993, *ApJ*, 415, 616, doi: [10.1086/173189](https://doi.org/10.1086/173189)
- Carr, J. S., Sellgren, K., & Balachandran, S. C. 2000, *ApJ*, 530, 307, doi: [10.1086/308340](https://doi.org/10.1086/308340)
- Chatzopoulos, S., Fritz, T. K., Gerhard, O., et al. 2015, *MNRAS*, 447, 948, doi: [10.1093/mnras/stu2452](https://doi.org/10.1093/mnras/stu2452)
- Chen, Z., Do, T., Ghez, A. M., et al. 2023, *ApJ*, 944, 79, doi: [10.3847/1538-4357/aca8ad](https://doi.org/10.3847/1538-4357/aca8ad)
- Cox, N. L. J., Cami, J., Kaper, L., et al. 2014, *A&A*, 569, A117, doi: [10.1051/0004-6361/201323061](https://doi.org/10.1051/0004-6361/201323061)
- Cunha, K., Sellgren, K., Smith, V. V., et al. 2007, *ApJ*, 669, 1011, doi: [10.1086/521813](https://doi.org/10.1086/521813)
- da Silva, L., Girardi, L., Pasquini, L., et al. 2006, *A&A*, 458, 609, doi: [10.1051/0004-6361:20065105](https://doi.org/10.1051/0004-6361:20065105)
- Delgado Mena, E., Moya, A., Adibekyan, V., et al. 2019, *A&A*, 624, A78, doi: [10.1051/0004-6361/201834783](https://doi.org/10.1051/0004-6361/201834783)
- Demarque, P., Woo, J.-H., Kim, Y.-C., & Yi, S. K. 2004, *ApJS*, 155, 667, doi: [10.1086/424966](https://doi.org/10.1086/424966)
- Di Matteo, P. 2016, *PASA*, 33, e027, doi: [10.1017/pasa.2016.11](https://doi.org/10.1017/pasa.2016.11)
- Do, T., Kerzendorf, W., Konopacky, Q., et al. 2018, *ApJL*, 855, L5, doi: [10.3847/2041-8213/aaac3](https://doi.org/10.3847/2041-8213/aaac3)
- Dong, H., Schödel, R., Williams, B. F., et al. 2017, *MNRAS*, 471, 3617, doi: [10.1093/mnras/stx1836](https://doi.org/10.1093/mnras/stx1836)
- Dotter, A. 2016, *ApJS*, 222, 8, doi: [10.3847/0067-0049/222/1/8](https://doi.org/10.3847/0067-0049/222/1/8)
- Ebenbichler, A., Postel, A., Przybilla, N., et al. 2022, *A&A*, 662, A81, doi: [10.1051/0004-6361/202142990](https://doi.org/10.1051/0004-6361/202142990)
- Elyajouri, M., Lallement, R., Monreal-Ibero, A., Capitanio, L., & Cox, N. L. J. 2017, *A&A*, 600, A129, doi: [10.1051/0004-6361/201630088](https://doi.org/10.1051/0004-6361/201630088)
- Feldmeier, A., Neumayer, N., Seth, A., et al. 2014, *A&A*, 570, A2, doi: [10.1051/0004-6361/201423777](https://doi.org/10.1051/0004-6361/201423777)
- Feldmeier-Krause, A., Kerzendorf, W., Neumayer, N., et al. 2017a, *MNRAS*, 464, 194, doi: [10.1093/mnras/stw2339](https://doi.org/10.1093/mnras/stw2339)
- Feldmeier-Krause, A., Zhu, L., Neumayer, N., et al. 2017b, *MNRAS*, 466, 4040, doi: [10.1093/mnras/stw3377](https://doi.org/10.1093/mnras/stw3377)
- Feldmeier-Krause, A., Neumayer, N., Schödel, R., et al. 2015, *A&A*, 584, A2, doi: [10.1051/0004-6361/201526336](https://doi.org/10.1051/0004-6361/201526336)

- Feldmeier-Krause, A., Kerzendorf, W., Do, T., et al. 2020, MNRAS, 494, 396, doi: [10.1093/mnras/staa703](https://doi.org/10.1093/mnras/staa703)
- Fragkoudi, F., Di Matteo, P., Haywood, M., et al. 2018, A&A, 616, A180, doi: [10.1051/0004-6361/201732509](https://doi.org/10.1051/0004-6361/201732509)
- Friske, J. K. S., & Schönrich, R. 2023, arXiv e-prints, arXiv:2310.01899, doi: [10.48550/arXiv.2310.01899](https://doi.org/10.48550/arXiv.2310.01899)
- Fritz, T. K., Chatzopoulos, S., Gerhard, O., et al. 2016, ApJ, 821, 44, doi: [10.3847/0004-637X/821/1/44](https://doi.org/10.3847/0004-637X/821/1/44)
- Galazutdinov, G. A., Lee, J.-J., Han, I., et al. 2017, MNRAS, 467, 3099, doi: [10.1093/mnras/stx330](https://doi.org/10.1093/mnras/stx330)
- Gallego-Cano, E., Fritz, T., Schödel, R., et al. 2024, A&A, 689, A190, doi: [10.1051/0004-6361/202449881](https://doi.org/10.1051/0004-6361/202449881)
- Gallego-Cano, E., Schödel, R., Noguera-Lara, F., et al. 2020, A&A, 634, A71, doi: [10.1051/0004-6361/201935303](https://doi.org/10.1051/0004-6361/201935303)
- Geballe, T. R. 2016, in Journal of Physics Conference Series, Vol. 728, Journal of Physics Conference Series, 062005, doi: [10.1088/1742-6596/728/6/062005](https://doi.org/10.1088/1742-6596/728/6/062005)
- Geballe, T. R., Najarro, F., Figer, D. F., Schlegelmilch, B. W., & La Fuente, D. 2011, Nature, 479, 200, doi: [10.1038/nature10527](https://doi.org/10.1038/nature10527)
- Gonzalez, O. A., Mucciarelli, A., Origlia, L., et al. 2020, The Messenger, 180, 18, doi: [10.18727/0722-6691/5196](https://doi.org/10.18727/0722-6691/5196)
- Gray, E. I., Read, J. I., Taylor, E., et al. 2024, arXiv e-prints, arXiv:2405.19286, doi: [10.48550/arXiv.2405.19286](https://doi.org/10.48550/arXiv.2405.19286)
- Grevesse, N., Asplund, M., & Sauval, A. J. 2007, SSRv, 130, 105, doi: [10.1007/s11214-007-9173-7](https://doi.org/10.1007/s11214-007-9173-7)
- Grisoni, V., Spitoni, E., Matteucci, F., et al. 2017, MNRAS, 472, 3637, doi: [10.1093/mnras/stx2201](https://doi.org/10.1093/mnras/stx2201)
- Guerço, R., Smith, V. V., Cunha, K., et al. 2022, MNRAS, 516, 2801, doi: [10.1093/mnras/stac2393](https://doi.org/10.1093/mnras/stac2393)
- Gully-Santiago, M., Wang, W., Deen, C., & Jaffe, D. 2012, in Society of Photo-Optical Instrumentation Engineers (SPIE) Conference Series, Vol. 8450, Modern Technologies in Space- and Ground-based Telescopes and Instrumentation II, ed. R. Navarro, C. R. Cunningham, & E. Prieto, 84502S, doi: [10.1117/12.926434](https://doi.org/10.1117/12.926434)
- Gustafsson, B., Edvardsson, B., Eriksson, K., et al. 2008, A&A, 486, 951
- Hamano, S., Kobayashi, N., Kawakita, H., et al. 2022, ApJS, 262, 2, doi: [10.3847/1538-4365/ac7567](https://doi.org/10.3847/1538-4365/ac7567)
- Han, J.-Y., Yuk, I.-S., Ko, K., et al. 2012, in Society of Photo-Optical Instrumentation Engineers (SPIE) Conference Series, Vol. 8550, Optical Systems Design 2012, ed. D. G. Smith, J.-L. M. Tissot, L. Mazuray, T. E. Kidger, F. Wyrowski, J. M. Raynor, R. Wartmann, S. David, A. Erdmann, A. P. Wood, P. Benítez, & M. C. de la Fuente, 85501B, doi: [10.1117/12.981169](https://doi.org/10.1117/12.981169)
- Hartmann, M., Debattista, V. P., Seth, A., Cappellari, M., & Quinn, T. R. 2011, MNRAS, 418, 2697, doi: [10.1111/j.1365-2966.2011.19659.x](https://doi.org/10.1111/j.1365-2966.2011.19659.x)
- Haywood, M., Di Matteo, P., Lehnert, M., et al. 2018, A&A, 618, A78, doi: [10.1051/0004-6361/201731363](https://doi.org/10.1051/0004-6361/201731363)
- Haywood, M., Di Matteo, P., Lehnert, M. D., Katz, D., & Gómez, A. 2013, A&A, 560, A109, doi: [10.1051/0004-6361/201321397](https://doi.org/10.1051/0004-6361/201321397)
- Henshaw, J. D., Barnes, A. T., Battersby, C., et al. 2023, in Astronomical Society of the Pacific Conference Series, Vol. 534, Protostars and Planets VII, ed. S. Inutsuka, Y. Aikawa, T. Muto, K. Tomida, & M. Tamura, 83, doi: [10.48550/arXiv.2203.11223](https://doi.org/10.48550/arXiv.2203.11223)
- Hidalgo, S. L., Pietrinferni, A., Cassisi, S., et al. 2018, ApJ, 856, 125, doi: [10.3847/1538-4357/aab158](https://doi.org/10.3847/1538-4357/aab158)
- Holtzman, J. A., Hasselquist, S., Shetrone, M., et al. 2018, AJ, 156, 125, doi: [10.3847/1538-3881/aad4f9](https://doi.org/10.3847/1538-3881/aad4f9)
- Hunter, J. D. 2007, Computing in Science and Engineering, 9, 90, doi: [10.1109/MCSE.2007.55](https://doi.org/10.1109/MCSE.2007.55)
- Jeong, U., Chun, M.-Y., Oh, J. S., et al. 2014, in Society of Photo-Optical Instrumentation Engineers (SPIE) Conference Series, Vol. 9154, High Energy, Optical, and Infrared Detectors for Astronomy VI, ed. A. D. Holland & J. Beletic, 91541X, doi: [10.1117/12.2055589](https://doi.org/10.1117/12.2055589)
- Johnson, C. I., Rich, R. M., Young, M. D., et al. 2020, MNRAS, 499, 2357, doi: [10.1093/mnras/staa2393](https://doi.org/10.1093/mnras/staa2393)
- Johnson, C. I., Rich, R. M., Simion, I. T., et al. 2022, MNRAS, 515, 1469, doi: [10.1093/mnras/stac1840](https://doi.org/10.1093/mnras/stac1840)
- Jönsson, H., Allende Prieto, C., Holtzman, J. A., et al. 2018, AJ, 156, 126, doi: [10.3847/1538-3881/aad4f5](https://doi.org/10.3847/1538-3881/aad4f5)
- Joyce, M., Johnson, C. I., Marchetti, T., et al. 2023, ApJ, 946, 28, doi: [10.3847/1538-4357/acb692](https://doi.org/10.3847/1538-4357/acb692)
- Kocher, J. 2024, Title
- Kordopatis, G., Wyse, R. F. G., Gilmore, G., et al. 2015, A&A, 582, A122, doi: [10.1051/0004-6361/201526258](https://doi.org/10.1051/0004-6361/201526258)
- Kordopatis, G., Schultheis, M., McMillan, P. J., et al. 2023, A&A, 669, A104, doi: [10.1051/0004-6361/202244283](https://doi.org/10.1051/0004-6361/202244283)
- Launhardt, R., Zylka, R., & Mezger, P. G. 2002, A&A, 384, 112, doi: [10.1051/0004-6361:20020017](https://doi.org/10.1051/0004-6361:20020017)
- Lee, J.-J., Gullikson, K., & Kaplan, K. 2017, Igrins/Plp 2.2.0, Zenodo, Zenodo, doi: [10.5281/zenodo.845059](https://doi.org/10.5281/zenodo.845059)
- Li, G., Gordon, I. E., Rothman, L. S., et al. 2015, ApJS, 216, 15, doi: [10.1088/0067-0049/216/1/15](https://doi.org/10.1088/0067-0049/216/1/15)
- Lim, D., Koch-Hansen, A. J., Chun, S.-H., Hong, S., & Lee, Y.-W. 2022, A&A, 666, A62, doi: [10.1051/0004-6361/202243877](https://doi.org/10.1051/0004-6361/202243877)
- Lomaeva, M., Jönsson, H., Ryde, N., Schultheis, M., & Thorsbro, B. 2019, A&A, 625, A141, doi: [10.1051/0004-6361/201834247](https://doi.org/10.1051/0004-6361/201834247)
- Mace, G., Sokal, K., Lee, J.-J., et al. 2018, in Society of Photo-Optical Instrumentation Engineers (SPIE) Conference Series, Vol. 10702, Ground-based and Airborne Instrumentation for Astronomy VII, ed. C. J. Evans, L. Simard, & H. Takami, 107020Q, doi: [10.1117/12.2312345](https://doi.org/10.1117/12.2312345)
- Manea, C., Hawkins, K., Ness, M. K., et al. 2023, arXiv e-prints, arXiv:2310.15257. <https://arxiv.org/abs/2310.15257>

- Mastrobuono-Battisti, A., & Capuzzo-Dolcetta, R. 2012, in *Astronomical Society of the Pacific Conference Series*, Vol. 453, *Advances in Computational Astrophysics: Methods, Tools, and Outcome*, ed. R. Capuzzo-Dolcetta, M. Limongi, & A. Tornambè, 237, doi: [10.48550/arXiv.1109.6620](https://doi.org/10.48550/arXiv.1109.6620)
- Matsunaga, N., Kawadu, T., Nishiyama, S., et al. 2011, *Nature*, 477, 188, doi: [10.1038/nature10359](https://doi.org/10.1038/nature10359)
- Matteucci, F. 2021, *A&A Rv*, 29, 5, doi: [10.1007/s00159-021-00133-8](https://doi.org/10.1007/s00159-021-00133-8)
- Matteucci, F., Grisoni, V., Spitoni, E., et al. 2019, *MNRAS*, 487, 5363, doi: [10.1093/mnras/stz1647](https://doi.org/10.1093/mnras/stz1647)
- Matteucci, F., Vasini, A., Grisoni, V., & Schultheis, M. 2020, *MNRAS*, 494, 5534, doi: [10.1093/mnras/staa1118](https://doi.org/10.1093/mnras/staa1118)
- McWilliam, A. 1997, *ARA&A*, 35, 503, doi: [10.1146/annurev.astro.35.1.503](https://doi.org/10.1146/annurev.astro.35.1.503)
- Meléndez, J., Asplund, M., Alves-Brito, A., et al. 2008, *A&A*, 484, L21, doi: [10.1051/0004-6361/200809398](https://doi.org/10.1051/0004-6361/200809398)
- Minniti, D., Lucas, P. W., Emerson, J. P., et al. 2010, *NewA*, 15, 433, doi: [10.1016/j.newast.2009.12.002](https://doi.org/10.1016/j.newast.2009.12.002)
- Moon, B., Wang, W., Park, C., et al. 2012, in *Society of Photo-Optical Instrumentation Engineers (SPIE) Conference Series*, Vol. 8450, *Modern Technologies in Space- and Ground-based Telescopes and Instrumentation II*, ed. R. Navarro, C. R. Cunningham, & E. Prieto, 845048, doi: [10.1117/12.925702](https://doi.org/10.1117/12.925702)
- Nandakumar, G., Ryde, N., Casagrande, L., & Mace, G. 2023, *A&A*, 675, A23, doi: [10.1051/0004-6361/202346149](https://doi.org/10.1051/0004-6361/202346149)
- Nandakumar, G., Ryde, N., Forsberg, R., et al. 2024a, *A&A*, 684, A15, doi: [10.1051/0004-6361/202348462](https://doi.org/10.1051/0004-6361/202348462)
- Nandakumar, G., Ryde, N., Schultheis, M., et al. 2018, *MNRAS*, 478, 4374, doi: [10.1093/mnras/sty1255](https://doi.org/10.1093/mnras/sty1255)
- Nandakumar, G., Ryde, N., Mace, G., et al. 2024b, *ApJ*, 964, 96, doi: [10.3847/1538-4357/ad22dc](https://doi.org/10.3847/1538-4357/ad22dc)
- Ness, M., Freeman, K., Athanassoula, E., et al. 2012, *ApJ*, 756, 22, doi: [10.1088/0004-637X/756/1/22](https://doi.org/10.1088/0004-637X/756/1/22)
- . 2013, *MNRAS*, 430, 836, doi: [10.1093/mnras/sts629](https://doi.org/10.1093/mnras/sts629)
- Neumayer, N., Seth, A., & Böker, T. 2020, *A&A Rv*, 28, 4, doi: [10.1007/s00159-020-00125-0](https://doi.org/10.1007/s00159-020-00125-0)
- Nieuwmunster, N., Nandakumar, G., Spitoni, E., et al. 2023, *A&A*, 671, A94, doi: [10.1051/0004-6361/202245374](https://doi.org/10.1051/0004-6361/202245374)
- Nieuwmunster, N., Schultheis, M., Sormani, M., et al. 2024, *A&A*, 685, A93, doi: [10.1051/0004-6361/202349000](https://doi.org/10.1051/0004-6361/202349000)
- Nishiyama, S., Nagata, T., Kusakabe, N., et al. 2006, *ApJ*, 638, 839, doi: [10.1086/499038](https://doi.org/10.1086/499038)
- Nishiyama, S., Yasui, K., Nagata, T., et al. 2013, *ApJL*, 769, L28, doi: [10.1088/2041-8205/769/2/L28](https://doi.org/10.1088/2041-8205/769/2/L28)
- Nogueras-Lara, F. 2022, *A&A*, 666, A72, doi: [10.1051/0004-6361/202244411](https://doi.org/10.1051/0004-6361/202244411)
- Nogueras-Lara, F., Schödel, R., & Neumayer, N. 2021a, *ApJ*, 920, 97, doi: [10.3847/1538-4357/ac185e](https://doi.org/10.3847/1538-4357/ac185e)
- . 2021b, *A&A*, 653, A133, doi: [10.1051/0004-6361/202140996](https://doi.org/10.1051/0004-6361/202140996)
- Nogueras-Lara, F., Gallego-Calvente, A. T., Dong, H., et al. 2018, *A&A*, 610, A83, doi: [10.1051/0004-6361/201732002](https://doi.org/10.1051/0004-6361/201732002)
- Nogueras-Lara, F., Schödel, R., Gallego-Calvente, A. T., et al. 2019, *A&A*, 631, A20, doi: [10.1051/0004-6361/201936263](https://doi.org/10.1051/0004-6361/201936263)
- . 2020, *Nature Astronomy*, 4, 377, doi: [10.1038/s41550-019-0967-9](https://doi.org/10.1038/s41550-019-0967-9)
- Nogueras-Lara, F., Feldmeier-Krause, A., Schödel, R., et al. 2023, *A&A*, 680, A75, doi: [10.1051/0004-6361/202347421](https://doi.org/10.1051/0004-6361/202347421)
- Oh, J. S., Park, C., Cha, S.-M., et al. 2014, in *Society of Photo-Optical Instrumentation Engineers (SPIE) Conference Series*, Vol. 9147, *Ground-based and Airborne Instrumentation for Astronomy V*, ed. S. K. Ramsay, I. S. McLean, & H. Takami, 914739, doi: [10.1117/12.2055651](https://doi.org/10.1117/12.2055651)
- Park, C., Jaffe, D. T., Yuk, I.-S., et al. 2014, in *Society of Photo-Optical Instrumentation Engineers (SPIE) Conference Series*, Vol. 9147, *Ground-based and Airborne Instrumentation for Astronomy V*, ed. S. K. Ramsay, I. S. McLean, & H. Takami, 91471D, doi: [10.1117/12.2056431](https://doi.org/10.1117/12.2056431)
- Polyansky, O. L., Kyuberis, A. A., Zobov, N. F., et al. 2018, *MNRAS*, 480, 2597, doi: [10.1093/mnras/sty1877](https://doi.org/10.1093/mnras/sty1877)
- Renaud, F., Agertz, O., Andersson, E. P., et al. 2021a, *MNRAS*, 503, 5868, doi: [10.1093/mnras/stab543](https://doi.org/10.1093/mnras/stab543)
- Renaud, F., Agertz, O., Read, J. I., et al. 2021b, *MNRAS*, 503, 5846, doi: [10.1093/mnras/stab250](https://doi.org/10.1093/mnras/stab250)
- Rich, R. M., Ryde, N., Thorsbro, B., et al. 2017, *AJ*, 154, 239, doi: [10.3847/1538-3881/aa970a](https://doi.org/10.3847/1538-3881/aa970a)
- Rodrigues, T. S., Girardi, L., Miglio, A., et al. 2014, *MNRAS*, 445, 2758, doi: [10.1093/mnras/stu1907](https://doi.org/10.1093/mnras/stu1907)
- Rodrigues, T. S., Bossini, D., Miglio, A., et al. 2017, *MNRAS*, 467, 1433, doi: [10.1093/mnras/stx120](https://doi.org/10.1093/mnras/stx120)
- Rojas-Arriagada, A., Recio-Blanco, A., de Laverny, P., et al. 2017, *A&A*, 601, A140, doi: [10.1051/0004-6361/201629160](https://doi.org/10.1051/0004-6361/201629160)
- Rojas-Arriagada, A., Zasowski, G., Schultheis, M., et al. 2020, *MNRAS*, 499, 1037, doi: [10.1093/mnras/staa2807](https://doi.org/10.1093/mnras/staa2807)
- Ryde, N., Fritz, T. K., Rich, R. M., et al. 2016a, *ApJ*, 831, 40, doi: [10.3847/0004-637X/831/1/40](https://doi.org/10.3847/0004-637X/831/1/40)
- Ryde, N., & Schultheis, M. 2015, *A&A*, 573, A14, doi: [10.1051/0004-6361/201424486](https://doi.org/10.1051/0004-6361/201424486)
- Ryde, N., Schultheis, M., Grieco, V., et al. 2016b, *AJ*, 151, 1, doi: [10.3847/0004-6256/151/1/1](https://doi.org/10.3847/0004-6256/151/1/1)
- Ryde, N., Gustafsson, B., Edvardsson, B., et al. 2010, *A&A*, 509, A20, doi: [10.1051/0004-6361/200912687](https://doi.org/10.1051/0004-6361/200912687)
- Sawczynec, E., Mace, G., Gully-Santiago, M., & Jaffe, D. 2022, in *American Astronomical Society Meeting Abstracts*, Vol. 54, *American Astronomical Society Meeting Abstracts*, 203.06
- Schödel, R., Feldmeier, A., Kunneriath, D., et al. 2014a, *A&A*, 566, A47, doi: [10.1051/0004-6361/201423481](https://doi.org/10.1051/0004-6361/201423481)

- Schödel, R., Feldmeier, A., Neumayer, N., Meyer, L., & Yelda, S. 2014b, *Classical and Quantum Gravity*, 31, 244007, doi: [10.1088/0264-9381/31/24/244007](https://doi.org/10.1088/0264-9381/31/24/244007)
- Schödel, R., Noguerras-Lara, F., Gallego-Cano, E., et al. 2020, *A&A*, 641, A102, doi: [10.1051/0004-6361/201936688](https://doi.org/10.1051/0004-6361/201936688)
- Schödel, R., Longmore, S., Henshaw, J., et al. 2023, arXiv e-prints, arXiv:2310.11912, doi: [10.48550/arXiv.2310.11912](https://doi.org/10.48550/arXiv.2310.11912)
- Schultheis, M., Cunha, K., Zasowski, G., et al. 2015, *A&A*, 584, A45, doi: [10.1051/0004-6361/201527027](https://doi.org/10.1051/0004-6361/201527027)
- Schultheis, M., Rojas-Arriagada, A., Cunha, K., et al. 2020, *A&A*, 642, A81, doi: [10.1051/0004-6361/202038327](https://doi.org/10.1051/0004-6361/202038327)
- Shen, J., Rich, R. M., Kormendy, J., et al. 2010, *ApJL*, 720, L72, doi: [10.1088/2041-8205/720/1/L72](https://doi.org/10.1088/2041-8205/720/1/L72)
- Smith, L. C., Lucas, P. W., Kurtev, R., et al. 2018, *MNRAS*, 474, 1826, doi: [10.1093/mnras/stx2789](https://doi.org/10.1093/mnras/stx2789)
- Snedden, C., Lucatello, S., Ram, R. S., Brooke, J. S. A., & Bernath, P. 2014, *ApJS*, 214, 26, doi: [10.1088/0067-0049/214/2/26](https://doi.org/10.1088/0067-0049/214/2/26)
- Sormani, M. C., Sanders, J. L., Fritz, T. K., et al. 2022, *MNRAS*, 512, 1857, doi: [10.1093/mnras/stac639](https://doi.org/10.1093/mnras/stac639)
- Soto, M., Rich, R. M., & Kuijken, K. 2007, *ApJL*, 665, L31, doi: [10.1086/521098](https://doi.org/10.1086/521098)
- Taylor, M. B. 2005, in *Astronomical Society of the Pacific Conference Series*, Vol. 347, *Astronomical Data Analysis Software and Systems XIV*, ed. P. Shopbell, M. Britton, & R. Ebert, 29
- Thorsbro, B., Ryde, N., Schultheis, M., et al. 2018, *ApJ*, 866, 52, doi: [10.3847/1538-4357/aadb97](https://doi.org/10.3847/1538-4357/aadb97)
- Thorsbro, B., Ryde, N., Rich, R. M., et al. 2020, *ApJ*, 894, 26, doi: [10.3847/1538-4357/ab8226](https://doi.org/10.3847/1538-4357/ab8226)
- Thorsbro, B., Forsberg, R., Kordopatis, G., et al. 2023, *ApJL*, 958, L18, doi: [10.3847/2041-8213/ad08b1](https://doi.org/10.3847/2041-8213/ad08b1)
- Tody, D. 1993, in *ASP Conf. Ser. 52: Astronomical Data Analysis Software and Systems II*, ed. R. J. Hanisch, R. J. V. Brissenden, & J. Barnes, 173
- Valenti, J. A., & Piskunov, N. 1996, *A&AS*, 118, 595
- . 2012, *SME: Spectroscopy Made Easy*. <http://ascl.net/1202.013>
- van der Walt, S., Colbert, S. C., & Varoquaux, G. 2011, *Computing in Science and Engineering*, 13, 22, doi: [10.1109/MCSE.2011.37](https://doi.org/10.1109/MCSE.2011.37)
- Vasiliev, E. 2019, *MNRAS*, 482, 1525, doi: [10.1093/mnras/sty2672](https://doi.org/10.1093/mnras/sty2672)
- Virtanen, P., Gommers, R., Oliphant, T. E., et al. 2020, *Nature Methods*, 17, 261, doi: [10.1038/s41592-019-0686-2](https://doi.org/10.1038/s41592-019-0686-2)
- Wang, W., Gully-Santiago, M., Deen, C., Mar, D. J., & Jaffe, D. T. 2010, in *Society of Photo-Optical Instrumentation Engineers (SPIE) Conference Series*, Vol. 7739, *Modern Technologies in Space- and Ground-based Telescopes and Instrumentation*, ed. E. Atad-Ettingui & D. Lemke, 77394L, doi: [10.1117/12.857164](https://doi.org/10.1117/12.857164)
- Woolley, S. E., & Weaver, T. A. 1995, *ApJS*, 101, 181, doi: [10.1086/192237](https://doi.org/10.1086/192237)
- Yuk, I.-S., Jaffe, D. T., Barnes, S., et al. 2010, in *Society of Photo-Optical Instrumentation Engineers (SPIE) Conference Series*, Vol. 7735, *Ground-based and Airborne Instrumentation for Astronomy III*, ed. I. S. McLean, S. K. Ramsay, & H. Takami, 77351M, doi: [10.1117/12.856864](https://doi.org/10.1117/12.856864)
- Zasowski, G., Ménard, B., Bizyaev, D., et al. 2015, *ApJ*, 798, 35, doi: [10.1088/0004-637X/798/1/35](https://doi.org/10.1088/0004-637X/798/1/35)
- Zasowski, G., Schultheis, M., Hasselquist, S., et al. 2019, *ApJ*, 870, 138, doi: [10.3847/1538-4357/aaeff4](https://doi.org/10.3847/1538-4357/aaeff4)
- Zoccali, M., Vasquez, S., Gonzalez, O. A., et al. 2017, *A&A*, 599, A12, doi: [10.1051/0004-6361/201629805](https://doi.org/10.1051/0004-6361/201629805)